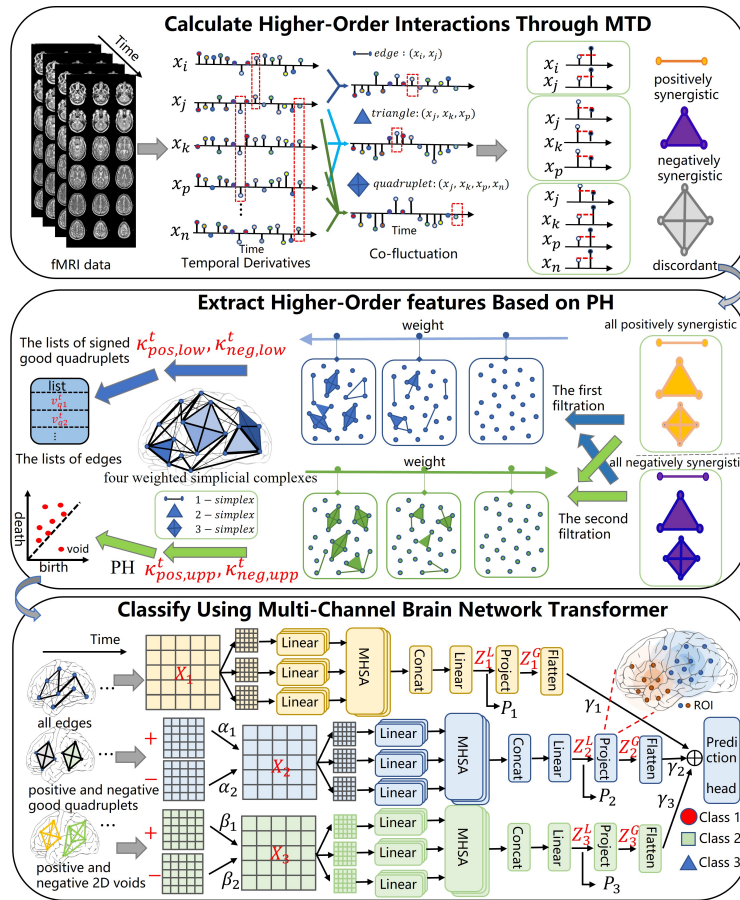


# Graphical Abstract

**HOI-Brain: a novel multi-channel transformers framework for brain disorder diagnosis by accurately extracting signed higher-order interactions from fMRI**

Dengyi Zhao, Zhiheng Zhou, Guiying Yan, Dongxiao Yu, Xingqin Qi



## Highlights

### **HOI-Brain: a novel multi-channel transformers framework for brain disorder diagnosis by accurately extracting signed higher-order interactions from fMRI**

Dengyi Zhao, Zhiheng Zhou, Guiying Yan, Dongxiao Yu, Xingqin Qi

- We propose the Multiplication of Temporal Derivatives (MTD), a novel metric designed to quantify dynamic functional co-fluctuations across group-level brain regions of interest.
- For the first time, we define the monotonic weighted simplicial complex for brain networks, extracting quadruplet-level interaction signatures and two-dimensional void descriptors via Persistent Homology.
- We propose the first to discriminate positive and negative synergistic higher-order interactions and reveal their disease-specific associations in brain disorders.
- We introduce a novel multi-channel brain network Transformer to synergistically integrate lower-order edge features with the higher-order topological invariants.
- We identify disease-stage-dependent higher-order organizational patterns, showing gradually weakened concordant higher-order interactions (HOIs) from healthy controls to AD/ASD patients, while revealing an opposite trend in Parkinson’s disease.

# HOI-Brain: a novel multi-channel transformers framework for brain disorder diagnosis by accurately extracting signed higher-order interactions from fMRI

Dengyi Zhao<sup>a</sup>, Zhiheng Zhou<sup>b</sup>, Guiying Yan<sup>b</sup>, Dongxiao Yu<sup>c</sup>, Xingqin Qi<sup>a,\*</sup>

<sup>a</sup>*School of Mathematics and Statistics,  
Shandong University, Weihai, 264209, Shandong, China*

<sup>b</sup>*Academy of Mathematics and Systems Science, Chinese Academy of  
Sciences, Beijing, 100190, Beijing, China*

<sup>c</sup>*School of Computer Science and Technology,  
Shandong University, Qingdao, 266000, Shandong, China*

---

## Abstract

Accurately characterizing the higher-order interactions of brain regions and effectively extracting the interpretable higher-order organizational patterns from functional Magnetic Resonance Imaging (fMRI) data are crucial for the diagnosis of brain diseases. However, current graph models mainly focus on pairwise patterns, as well as triadic patterns within brain while overlooking more higher-order patterns with signs, limiting an integrated understanding of brain-wide communication. To address these challenges, we propose HOI-Brain (Higher-Order Interaction in Brain Network), a novel computational framework that enables the utilization of signed higher-order interactions and signed organizational patterns in fMRI data for the diagnosis of brain diseases. Specifically, we present a new calculation of co-fluctuations based on Multiplication of Temporal Derivatives to detect higher-order interactions with adequate temporal resolution. Next, we further distinguish positively and negatively synergistic higher-order interactions and encode them in the monotonic weighted simplicial complexes, which can offer detailed insights into the communication within the brain. Moreover, we employ Persistent

---

\*Corresponding author.

*Email addresses:* zhaodengyi@mail.sdu.edu.cn (Dengyi Zhao),  
zhouzhiheng@amss.ac.cn (Zhiheng Zhou), yangy@amt.ac.cn (Guiying Yan),  
dxyu@sdu.edu.cn (Dongxiao Yu), qixingqin@sdu.edu.cn (Xingqin Qi)

Homology in the monotonic weighted simplicial complexes of the brain to extract signed higher-dimensional neural organisations from a spatiotemporal perspective. Finally, a multi-channel transformers architecture is proposed to holistically integrate information from heterogeneous topological features. Comprehensive experiments across Alzheimer’s disease (AD), Parkinson’s disease (PD), and Autism Spectrum Disorder (ASD) datasets demonstrate the superiority, effectiveness, and interpretability of our framework. The identified key brain regions and higher-order patterns consistently align with neuroscientific evidence, showing concordant HOIs weakening in the brain of AD/ASD but enhancement in PD, offering mechanistic insights into these brain disorders. Our code is available.

*Keywords:* Brain network, higher-order interaction, Transformer, fMRI biomarker, Persistent Homology theory

---

## 1. Introduction

Functional magnetic resonance imaging (fMRI) represents a pivotal instrument in the field of neuroscience, serving to identify potential neuroimaging biomarkers. These biomarkers are instrumental in the automated diagnosis of various brain disorders, including Alzheimer’s disease (AD), autism spectrum disorder (ASD), and Parkinson’s disease (PD) (Lindquist, 2008; Fornito et al., 2016). Specifically, resting state fMRI measures functional connectivity between brain regions via blood-oxygen-level-dependent (BOLD) signals. This process naturally models the brain as a network, defining regions of interest (ROIs) as nodes and functional connections between ROIs as edges (Sporns, 2010; Bullmore and Sporns, 2009). Abnormalities in this network at the whole-brain level are hypothesised to yield disease-related biomarker signatures (Wang et al., 2021).

A significant number of graph data mining methodologies are then applied to such brain networks for brain disorder diagnosis, with the goal of understanding and analysing the elements and interactions of neurological systems from a network perspective. Examples of such models include graph neural network (GNN)-based models (Xia et al., 2025), brain Transformer-based models (Kan et al., 2022b), hypergraph neural network (HGNN)-based models (Wang et al., 2024a), and Persistent Homology (PH)-based models (Bian et al., 2023). Despite the evidence from these studies demonstrating the considerable potential of network-based approaches to elucidating the

complexities of the brain and diagnosing brain disorders, graph analysis of brain networks remains an emerging field in its infancy (Fotiadis et al., 2024).

In recent developments, graph neural network (GNN) techniques have been employed to analyse brain networks characterised by pairwise interactions. The utilisation of these methodologies enables the extraction of potential topological features, which are instrumental in the diagnosis of brain disorders (Luo et al., 2024). A number of GNN-based models have been proposed for brain networks, including GroupINN (Yan et al., 2019), BrainGNN (Li et al., 2021), FBNetGen (Kan et al., 2022a), BPI-GNN (Zheng et al., 2024), and ASD-HNet (Luo et al., 2025). These models have demonstrated the potential to achieve favourable diagnostic performance. It is widely accepted that GNN-based models utilise a message passing mechanism, whereby the embedding of a brain ROI is updated by aggregating information from its neighbouring ROIs. This process facilitates the learning of a discriminative graph-level representation of the brain connectivity network. However, these methods are limited by the underlying assumption that interactions between nodes are strictly two-way. Recent studies have indicated a growing body of evidence that suggests the complexity of brain-region interactions extends far beyond the established pairwise connections. There is now a growing consensus that widespread co-fluctuations occur in groups of nodes that evolve over time (Battiston et al., 2020; Chelaru et al., 2021). Consequently, the limited expressiveness of traditional GNNs prevents them from capturing higher-order interactions (HOIs) in brain networks, and the topological features they extract are typically regarded as lower-order.

Transformer-based brain network models have achieved considerable success in the diagnosis of brain disorders, due to their capacity to capture global patterns. Representative examples include Graph Transformer (Ying et al., 2021), Brain Network Transformer (Kan et al., 2022b), TSEN (Hu et al., 2023), and Long-range Brain Transformer (Yu et al., 2024). It is evident that these models naturally construct fully connected graphs and, through a powerful global attention mechanism, adaptively learn pairwise interaction relationships for brain disorder diagnosis. However, the prevailing approach involves the utilisation of either the raw time series features of brain regions or the functional connectivity matrix as node-level input, thereby overlooking significant higher-order topological information among ROIs.

A number of studies have concentrated on the representation of HOIs in brain networks using more sophisticated models, with a particular focus on hypergraphs. This approach has been shown to enhance diagnostic per-

formance for brain diseases, as evidenced by citations in the literature (Jie et al., 2016; Xiao et al., 2019; Wang et al., 2022; Hao et al., 2023; Wang et al., 2024a). Despite the encouraging outcomes demonstrated by HGNN-based models in characterising HOIs through hyperedges generated via  $k$ -nearest neighbour or  $k$ -hop neighbourhoods, this node-centric construction scheme appears to be incompatible with the concept of group dependence. This is due to its inability to capture authentic simultaneous interactions among groups of ROIs. Furthermore, it has been demonstrated that higher-order features extracted by HGNN-based models can obscure their relationship to specific topological or neurobiological phenomena (Kim et al., 2024; Su et al., 2024).

In order to extract higher-order topological features that are more readily interpretable for the purpose of brain-disorder diagnosis, recent studies have adopted Persistent Homology, a topological approach capable of reconstructing HOI structures and delivering state-of-the-art performance in characterising brain topological profiles (Hyekyoung et al., 2011; Sizemore et al., 2018). However, the majority of investigations into higher-order structures in brain networks have focused on 0-dimensional (connected components) and 1-dimensional (cycles) topological profiles formed by nodes and edges. These dimensions do not link HOIs in the brain to higher-order organisations that would provide a truly higher-dimensional perspective (Talesh Jafadideh and Mohammadzadeh Asl, 2022; Bian et al., 2024; Bhattacharya et al., 2025). In order to address the aforementioned limitation, researchers have recently employed synchronisation phenomena to construct more accurate simplicial complexes for modelling HOIs. Furthermore, they have utilised Persistent Homology to capture 1-dimensional cycles that reflect triplet interactions (Santoro et al., 2024). Comprehensive analyses demonstrate that methods incorporating inferred HOIs among three ROIs outperform traditional pairwise approaches, thereby offering new insights into the higher-order organisation of fMRI time-series data. Nonetheless, the extant evidence indicates that triplet interactions can be decomposed into linear combinations of pairwise interactions, provided that said interactions are linearly decomposable. This finding suggests that some triplets may not in fact represent genuine higher-order phenomena (Delabays et al., 2025; Neuhäuser et al., 2020). Consequently, consideration of HOIs and organisational structures may offer a more profound comprehension of brain function. Furthermore, extant measures of instantaneous co-fluctuation are contingent on extended Pearson correlation, a method that is deficient in temporal resolution when it comes to

detecting spatiotemporal interactions among groups of regions (Shine et al., 2015). Finally, the role of signed HOIs, which have the potential to provide valuable diagnostic information in cases of neurological conditions, has been largely overlooked in these studies.

In order to address the methodological challenges identified, a novel computational framework has been proposed in this paper. As shown in Figure 1, this framework, designated HOI-Brain (Higher-Order Interactions in Brain), facilitates a comprehensive analysis of HOIs in fMRI data.

Firstly, a novel metric – Multiplication of Temporal Derivatives (MTD) – is introduced with the aim of quantifying dynamic functional co-fluctuations among groups of ROIs. MTD performs element-wise product calculations on the temporal derivatives of blood-oxygen-level-dependent (BOLD) signals, thereby yielding instantaneous co-fluctuation magnitudes for  $k$ -node interactions. This approach will offer a more reliable means of identifying genuine higher-order neural interactions in comparison to Pearson’s correlation.

Secondly, we further divided concordant interactions into two distinct groups: those exhibiting positive synergy and those exhibiting negative synergy. Positively synergistic interactions are indicative of multiple brain regions that exhibit simultaneous activation at a given moment relative to the preceding one, while negatively synergistic interactions indicate that these regions collectively exhibit inhibition at the current moment compared to the prior moment. Collectively, these interactions offer detailed information about complex coordination and communication within the brain, thus improving the effectiveness of brain disease diagnosis. Our study explores the influence of signed HOIs using the self-attention mechanism.

Thirdly, adopting a spatiotemporal analytic perspective, we encode these signed co-fluctuations into the monotonic weighted simplicial complexes. These complexes link instantaneous co-fluctuation of  $k$ -node interactions in the brain to the weight of the  $k$ -simplex. This facilitates the accommodation of more information about interactions among multiple ROIs in comparison to pairwise networks. The extraction of four types signed of higher-order topological which from these monotonic weighted simplicial complexes are based on Persistent Homology theory. The first type of interaction signature is positive and negative quadruplet-level interaction signatures. These capture irreducible higher-order neural coordination patterns. The second type of interaction signature is positive and negative two-dimensional void descriptors. These characterise the intrinsic geometric organisation of neural activity from a higher-dimensional manifold perspective.

Then, given the significance of both lower-order interactions (LOIs) and HOIs in brain network analysis tasks, a multi-channel brain network Transformer is developed to synergistically integrate lower-order edge features with the above four types of higher-order topological invariants. Specifically, higher-order information is injected into a multi-channel Transformer, and an orthonormal clustering readout operation is employed. This operation is based on self-supervised soft clustering and orthonormal projection, and it is used to learn distinguishable cluster-aware lower- and higher-order node embeddings. Subsequently, an attention mechanism is employed to facilitate the adaptive fusion of features encoded by disparate channels. Finally, the Multi-Layer Perceptron (MLP) is employed as the prediction head to categorise the various levels of topological features that have been extracted from the multi-channel brain network Transformer.

Experiments on Alzheimer’s disease, autism spectrum disorder, and Parkinson’s disease datasets have demonstrated its superiority over 20 state-of-the-art baselines. The present study employs an ablation approach to demonstrate the significance of higher-order topological features, the efficacy of distinct components of the proposed model, and the superiority of quadruplet interactions over triplet interactions in enhancing the diagnostic efficacy of brain diseases. In the subsequent stage of the research, the importance of signed information and channel information was identified by means of visualising the attention scores in the self-attention mechanism. This finding indicates that the integration of positive and negative information, in conjunction with higher-order and low-order interactions within brain networks, can remarkably enhance diagnostic performance in a range of brain disease diagnostic tasks. By visualising the self-attention maps in the multi-channel brain network Transformer, interaction patterns among disease-related key brain regions and key interactions between ROIs were identified from a more comprehensive brain network perspective. Furthermore, we have identified higher-order organisational patterns associated with specific stages of disease progression, based on the methods employed.

In general, this study makes four contributions.

1. We propose a novel metric - Multiplication of Temporal Derivatives (MTD) - for quantifying dynamic functional co-fluctuations of group ROIs. This approach employs element-wise products of temporal derivatives of blood oxygen level-dependent (BOLD) signals to represent instantaneous co-fluctuation magnitudes of  $k$ -node interactions, which

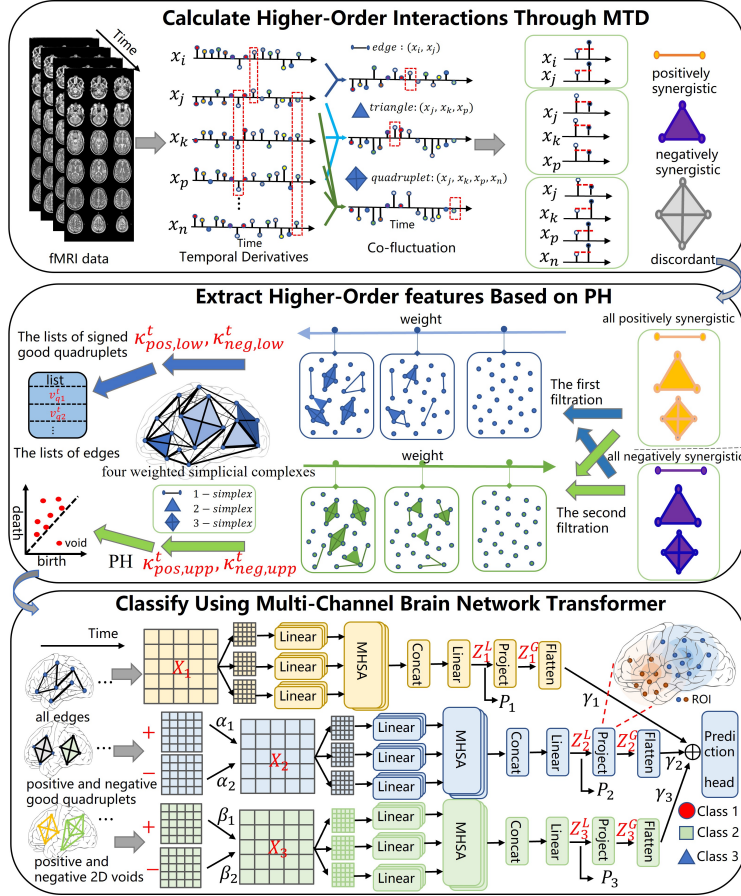


Figure 1: Overall framework of HOI-Brain. Individual fMRI data are transformed into  $N$  original fMRI signals through a preprocessing pipeline. A novel metric - Multiplication of Temporal Derivatives (MTD) - is used to quantify dynamic functional co-fluctuations of group ROIs. Then, at each timepoint  $t$ , some instantaneous  $k$ -order co-fluctuation are encoded into four signed monotonic weighted simplicial complexes based on filtrations, respectively. Persistent Homology is applied to analyze these signed monotonic weighted simplicial complexes at each  $t$ . Five feature matrices are generated by extracting all edges, signed good quadruplets, and signed 2D voids. These matrices are temporally averaged across all timepoints to stabilize feature representations. By incorporating the lower-order and higher-order feature, a multi-channel brain network Transformer is used to produce the final classification.

can achieve reliable identification of genuine higher-order neural interactions compared to Pearson correlation.

2. For the first time, we define the monotonic weighted simplicial complex for brain networks, extracting quadruplet-level interaction signatures and two-dimensional void descriptors via persistent homology. This provides a higher-dimensional perspective for studying higher-order brain structures compared to one-dimensional cycles.
3. To the best of our knowledge, this is the first attempt to distinguish between positively and negatively synergistic HOIs, which may offer valuable insights into the complex coordination and communication within the brain, thereby improving the effectiveness of brain disease diagnosis.
4. We propose a novel multi-channel brain network Transformer to synergistically integrate lower-order edge features with the higher-order topological invariants.
5. We identify disease-stage-dependent higher-order organizational patterns, showing gradually weakened concordant HOIs from healthy controls to AD/ASD patients, while revealing an opposite trend in Parkinson’s disease.

The contributions made in this work illustrate the potential of quadruplet or greater-order region interactions in improving the diagnostic efficacy of brain diseases and advancing the understanding of brain networks and neurodegenerative diseases.

## 2. Related work

### 2.1. Graph Models Based on Deep Learning

A significant number of graph models are then applied to brain networks for the purpose of brain disorder diagnosis, with the objective being to understand and analyse the elements and interactions of neurological systems from a network perspective. Graph neural networks (GNNs) have been demonstrated to be particularly effective in modelling brain connectomes, due to their ability to effectively capture subtle, latent representations and nonlinear relationships in graph-structured data. A number of GNN-based models, specifically designed for brain networks, have been proposed, and these have achieved a promising diagnostic performance. For instance, GroupINN

(Yan et al., 2019) incorporates the concept of node grouping into the neural network and designs a random-walk-based variant of graph convolutional layer. BrainGNN (Li et al., 2021) has developed a novel ROI-aware graph convolutional (Ra-GConv) layer that utilises the topological and functional information of fMRI. FBNETGEN (Kan et al., 2022a) employs a task-aware GNN-based framework for fMRI analysis via functional brain network generation, which generates the brain connectivity matrices and predicts clinical outcomes simultaneously from fMRI BOLD signal series. BPI-GNN (Zheng et al., 2024) utilises the prototype learning method to analyse fMRI. ASD-HNNet (Luo et al., 2025) is a hybrid neural network model for the identification of autism spectrum disorder (ASD). This model extracts features from functional brain networks at three distinct levels: local ROI, community, and global representation. However, these methodologies are fundamentally predicated on a two-way network to model pairwise interactions and mine low-order topological features for the diagnosis of brain disorders, overlooking the influence of HOIs in the brain.

Furthermore, with the advent of sophisticated large language models, Transformer-based methodologies are being increasingly incorporated into brain graph structures. The Graph Transformer (Ying et al., 2021), a sophisticated machine learning algorithm, can be applied to brain networks to learn the strength of the connections between ROIs across individuals. Subsequently, the Brain Network Transformer (BNT) (Kan et al., 2022b) employs the distinctive characteristics inherent in brain network data to maximise the efficacy of Transformer-based models for brain network analysis, thereby circumventing the necessity for time-consuming computations of eigenvalues or eigenvectors. TSEN (Hu et al., 2023) pioneered the incorporation of snowball graph convolution as position embedding within the Transformer structure, a methodology that has been proven to be both straightforward and efficacious in the context of capturing local patterns of brain activity in a natural manner. Long-range Brain Transformer (Yu et al., 2024) injects the long-range embeddings into a Transformer framework, integrating both short-range and long-range dependencies between ROIs using the self-attention mechanism. It is evident that these works disregard substantial higher-order topological information among ROIs.

A number of studies have been conducted on the construction of HOIs in the brain with a view to enhancing the performance of brain disorder diagnosis based on hypergraphs. For instance, a novel framework is proposed to estimate the hyper-connectivity network of brain functions for the diagno-

sis of brain disease (Jie et al., 2016). MHL-Hypergraph (Xiao et al., 2019) proposes a multi-hypergraph learning-based method to compute a unified hypergraph similarity matrix from multi-paradigm fMRI data to represent an FCN for each subject. An evolving hypergraph convolutional network (Wang et al., 2022) for the dynamic hyper-brain network is proposed, which adds the attention mechanism to further enhance the ability of representation learning. In order to take the temporal characteristics of longitudinal data into consideration, a weighted hypergraph convolution network (WHGCN) has been designed to utilise the internal correlations among different time points and to leverage higher-order relationships between subjects for the purpose of AD detection (Hao et al., 2023). CcSi-MHAHGEL (Wang et al., 2024a) pioneered a novel hypergraph convolution network framework for extracting multiatlas-based FCN embeddings, with the objective of facilitating multisite ASD identification. In this framework, hyperedge-aware HGCN was developed to capture complex higher-order information in brain networks. The majority of these studies employ  $k$ -nearest neighbour or  $k$ -hop neighbour constructions in order to generate hypergraphs. However, it has been demonstrated that these constructions are inconsistent with the definition of group dependence in brain regions. Moreover, higher-order features extracted using hypergraph neural networks (HGNNs) are frequently regarded as being less interpretable.

## 2.2. Persistent Homology on Brain Connectome

Persistent homology (PH) is a widely utilised, effective algebraic topological tool for the analysis of the brain connectome, enabling the capture of more interpretable, higher-order topological features. In lieu of endeavouring to ascertain a solitary optimum threshold, researchers (Hyekyoung et al., 2011) propose the examination of the topological changes in the brain network as the threshold is increased continuously, based on Persistent Homology. Researchers (Sizemore et al., 2018) also highlight the importance of cliques and cavities in the human connectome, and locate topological cavities of different dimensions, around which information may flow in either diverging or converging patterns. In order to address the challenging issue of comparing functional connectivity networks (FCNs) across different spatiotemporal resolutions, researchers (Cassidy et al., 2018) have developed a novel network comparison framework based on Persistent Homology. The purpose of this framework is to observe the change of 0-dimensional homology groups. Furthermore, researchers (Bian et al., 2024) propose an adversarially trained

Persistent Homology-based graph convolutional network (ATPGCN) to capture disease-specific brain connectome patterns for brain disorder diagnosis. Researchers (Bhattacharya et al., 2025) utilise the persistent topological features of connected components  $H_0$  and loops  $H_1$  for the identification of brain disorders, which are quantified by two methods: Vietoris-Rips filtration and graph filtration. Nevertheless, the aforementioned studies have overlooked the significance of two-dimensional topological profiles (i.e., voids) and have failed to establish a correlation between HOIs in the brain and these higher-order organisations. Recently, researchers (Santoro et al., 2024) have adopted certain methodologies grounded in the synchronisation phenomenon to construct more accurate simplicial complexes for modeling HOIs and use PH to capture 1-dimensional cycles related to triplet interactions. However, this can easily generate a large number of false positive HOIs and overlook higher-order quadruplet interactions with adequate temporal resolution. Besides, the influence of signed HOIs was overlooked in these studies, which could offer a broader diagnostic view of neurological conditions.

### 3. Preliminaries

In this section, we firstly present the problem formulation of this paper. Then, we propose a general method for mining HOIs in time series data using Multiplication of Temporal Derivatives. Finally, we introduce a new definition of monotonic weighted simplicial complex. These will provide the theoretical basis for the methods of brain disease diagnosis in the following text.

#### 3.1. Problem Formulation

The task of diagnosing brain disorders primarily involves inferring specific properties (represented as class labels) from fMRI data in the form of graphs. Given a labeled dataset  $\mathcal{D} = \{(\mathcal{G}, \mathcal{Y})\} = \{(G_i, y_i)\}_{i=1}^N$ , where each graph  $G_i \in \mathcal{G}$  corresponds to a label  $y_i \in \mathcal{Y}$ , the goal is to extract features to train a mapping function  $f_\theta : \mathcal{G} \rightarrow \mathcal{Y}$  that generalizes to unobserved graphs. For example, in studies of Alzheimer’s disease using brain networks, the label space comprises three diagnostic categories: CN (Cognitively Normal), MCI (Mild Cognitive Impairment) and AD (Alzheimer’s Disease). The objective is to extract both lower-order and higher-order topological features from annotated brain network data in order to learn a robust classifier  $f_\theta$ , ensuring its effectiveness on novel, unseen brain connectomes.

### 3.2. Multiplication of Temporal Derivatives for Processing Multivariate Time Series

To better capture HOIs in multivariate time series data with adequate temporal resolution, we propose a novel method for estimating instantaneous co-fluctuation magnitudes between several variables.

Let  $\mathbf{x}_i = [x_i(1), x_i(2), \dots, x_i(T)]$  represent the generic time series recorded from variable  $i$ . We first calculate the temporal derivative  $\dot{x}_i$  of each time series  $\mathbf{x}_i$  by performing a first-order differencing:

$$\dot{x}_i(t-1) = x_i(t) - x_i(t-1) \quad (1)$$

for  $t = 2, 3, \dots, T$ . Then we normalize each data point by dividing the temporal derivative  $\dot{x}_i(t)$  by its standard deviation  $\sigma_{\dot{x}_i}$ , computed over the entire time course. This normalization yields the new time series  $q_i(t)$  as:

$$q_i(t) = \frac{\dot{x}_i(t)}{\sigma_{\dot{x}_i}} \quad (2)$$

Then the new representing vector for the  $i$ th variable is denoted as  $\mathbf{q}_i$ .

Subsequently, the generic element at time  $t$  of the  $z$ -scored  $k$ -order co-fluctuation among  $k+1$  new time series is calculated as:

$$\xi_{0\dots k}(t) = \frac{\prod_{m=0}^k q_m(t) - \mu \left[ \bigodot_{m=0}^k \mathbf{q}_m \right]}{\sigma \left[ \bigodot_{m=0}^k \mathbf{q}_m \right]}, \quad (3)$$

where  $\mu[\cdot]$  and  $\sigma[\cdot]$  represent the time-averaged mean and standard deviation functions, respectively;  $\prod$  denotes the product of the elements;  $\bigodot$  represents the element-wise product of vectors.

To differentiate concordant group interactions from discordant ones in a  $k$ -order product, concordant signs are always positively mapped, while discordant signs are negatively mapped. Formally,

$$\text{sign} [\xi_{0\dots k}(t)] = \begin{cases} +1 & \text{if } q_0(t), \dots, q_k(t) \text{ are all non-negative or non-positive,} \\ -1 & \text{otherwise.} \end{cases} \quad (4)$$

In other words, the weight  $w_{0\dots k}(t)$  at time  $t$  of the  $k$ -order co-fluctuations is defined as

$$w_{0\dots k}(t) = \text{sign} [\xi_{0\dots k}(t)] |\xi_{0\dots k}(t)|. \quad (5)$$

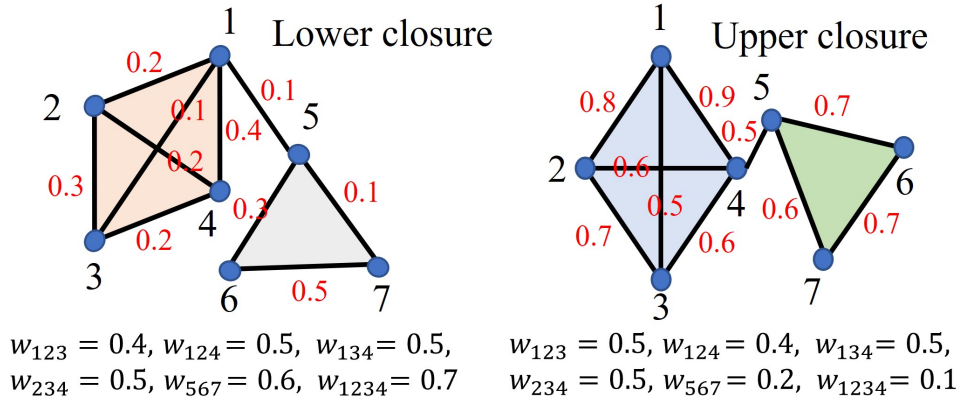


Figure 2: The illustration shows two types of monotonic weighted simplicial complexes on the left that satisfy the lower closure condition, and one on the right that satisfies the upper closure condition. The red numbers represent the weights of 1-simplices, and the text below indicates the weights of 2-simplices and 3-simplices.

It is noteworthy that our proposed method, by computing the product of first-order difference sequences of multivariate time series, enables the investigation of higher-order dynamic interactions, thereby providing a viable approach for exploring complex nonlinear coupling mechanisms in multivariate time series data.

### 3.3. The Monotonic Weighted Simplicial Complex

**Definition 1. (*Simplicial Complex*)** An abstract simplicial complex  $\mathcal{K}$  on a finite vertex set  $V$  is a collection of some non-empty subsets of  $V$  satisfying:

1. For every  $v \in V$ , the singleton  $\{v\}$  belongs to  $\mathcal{K}$ .
2. If  $\sigma \in \mathcal{K}$  and  $\tau \subseteq \sigma$  is a non-empty subset, then  $\tau \in \mathcal{K}$ .

Each element  $\sigma \in \mathcal{K}$  is called a simplex. A simplex with  $|\sigma| = k + 1$  vertices is a  $k$ -simplex, representing a  $k$ -order interaction. A subset  $\tau \subseteq \sigma$  satisfying  $|\tau| = k$  is called a *face* of  $\sigma$ .

Previous studies assigned arbitrary weights to simplices without imposing closure conditions on the weights (Baccini et al., 2022). To explore some special higher-order structures in the simplicial complex, here we propose a new definition of weighted simplicial complexes.

**Definition 2. (*Monotonic Weighted Simplicial Complex*)** Let  $\mathcal{K}$  be an abstract simplicial complex on vertex set  $V$ , where each simplex  $\sigma \in \mathcal{K}$  is a non-empty finite subset of  $V$ . A monotonic weighted simplicial complex is a pair  $(\mathcal{K}, w)$  with a weight function  $w : \mathcal{K} \rightarrow \mathbb{R}$  satisfying the following lower closure condition:

- (**Lower closure**) For any  $\sigma \in \mathcal{K}$ , any face  $\tau \subseteq \sigma$ ,  $w(\tau) \leq w(\sigma)$ .

In addition, a monotonic weighted simplicial complex is also a pair  $(\mathcal{K}, w)$  with a weight function  $w : \mathcal{K} \rightarrow \mathbb{R}$  satisfying the following upper closure condition:

- (**Upper closure**) For any  $\sigma \in \mathcal{K}$ , any face  $\tau \subseteq \sigma$ ,  $w(\tau) \geq w(\sigma)$ .

As shown in Figure 2, it shows two types of monotonic weighted simplicial complexes. The new definition allows us to explore some special higher-order structures satisfying the monotonicity closure conditions in the weighted simplicial complex, providing new insights.

## 4. Method

In this section, we introduce the method of HOI-Brain for diagnosing brain diseases, which captures signed high-order interactions and signed higher-order organizational patterns in fMRI data. HOI-Brain consists of four parts: calculating signed high-order interactions through Multiplication of Temporal Derivatives, constructing monotonic weighted simplicial complexes, extracting higher-order and low-order organizations in fMRI data, and classifying with a multi-channel brain network Transformer.

### 4.1. Calculate Signed Higher-Order Interactions Through Multiplication of Temporal Derivatives.

Recently, some computational methods have focused on capturing dynamic higher-order interactions in the brain (Faskowitz et al., 2020; Santoro et al., 2023, 2024), but these methods based on extended Pearson correlation have generally been limited by the lack of adequate temporal resolution, especially when capturing more higher-order interactions, such as quadruplets (Shine et al., 2015). To better capture higher-order interactions in the brain, we utilize the designed Multiplication of Temporal Derivatives on fMRI data, which is described in Section 3.2.

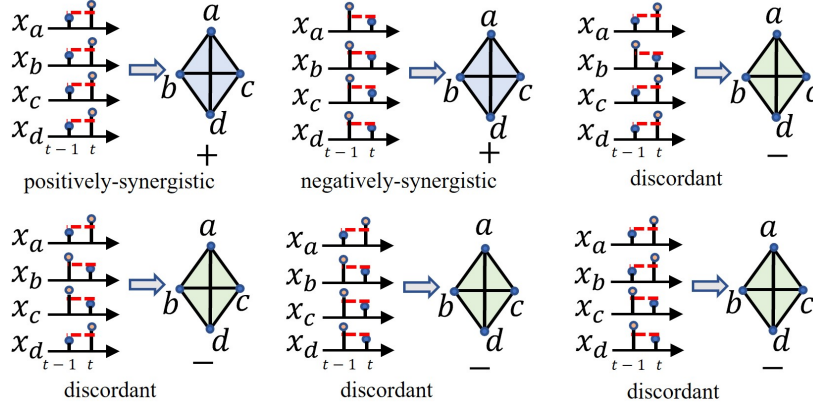


Figure 3: The illustration of six different signed quadruplet higher-order interactions. We exclusively focus on the first two types of signed quadruplet higher-order interactions with the concordant positive signs.

In particular, individual fMRI data are transformed into  $N$  original fMRI signals through a preprocessing pipeline. Temporal derivatives of each time series (length  $t$ ) are computed via first-order differencing, followed by normalization where each derivative is divided by its standard deviation across the entire time course. All possible  $k$ -order time series are generated by element-wise products of  $k+1$  normalized time series. These series are further z-scored to ensure cross- $k$ -order comparability. These  $k$ -order time series represent instantaneous co-fluctuation magnitudes of  $(k+1)$ -node interactions (e.g., edges, triangles, quadruplets).

If we compute all possible products up to order  $k$ , this will result in  $\binom{N}{k+1}$  different co-fluctuation time series for each order  $k$ . In this paper, we focus on co-fluctuations up to dimension  $k=3$  to capture quadruplet interactions. In this way, the Multiplication of Temporal Derivatives allows us to clarify the precise dynamic relationships among ROIs with better temporal precision than Pearson correlation coefficients.

It is important to acknowledge that for all  $k$ -order co-fluctuations, there exist two categories of signs for co-fluctuations: concordant signs and discordant signs, as shown in Figure 3. This study focuses exclusively on concordant signs, eschewing the examination of discordant signs. This is due to the potential for discordant signs to represent a confusing redundancy of information across multiple brain regions (Santoro et al., 2023). The concordant interactions were subsequently categorised into two distinct groups:

**1) Positively synergistic interactions** are indicative of multiple brain regions that exhibit simultaneous activation at a given moment relative to the preceding one. These interactions are mathematically defined by the conditions:

$$w_{i_0 i_1 \dots i_k} > 0 \quad \text{and} \quad q_{i_0} > 0, q_{i_1} > 0, \dots, q_{i_k} > 0 \quad (6)$$

where  $w_{i_0 i_1 \dots i_k}$  denotes the weight assigned to the  $k$ -simplex  $\sigma = \{i_0, i_1, \dots, i_k\}$ ,  $q_{i_j}$  denotes the first-order temporal difference of the activity value at node  $i_j$ . Let  $S^+$  denote the set of all  $k$ -order positively synergistic interactions ( $k < 4$ ), with their weights  $w^+$ .

**2) Negatively synergistic interactions** indicate that these regions collectively exhibit inhibition at the current moment compared to the prior moment. These interactions are mathematically defined by the conditions:

$$w_{i_0 i_1 \dots i_k} > 0 \quad \text{and} \quad q_{i_0} < 0, q_{i_1} < 0, \dots, q_{i_k} < 0 \quad (7)$$

where  $w_{i_0 i_1 \dots i_k}$  denotes the weight assigned to the  $k$ -simplex  $\sigma = \{i_0, i_1, \dots, i_k\}$ ,  $q_{i_j}$  denotes the first-order temporal difference of the activity value at node  $i_j$ . Let  $S^-$  denote the set of all  $k$ -order negatively synergistic interactions ( $k < 4$ ), with their weights  $w^-$ .

Collectively, distinguishing these interactions can offer valuable insights into the complex coordination and communication within the brain, thus improving the effectiveness of brain disease diagnosis.

#### 4.2. Construct Monotonic Weighted Simplicial Complexes

Recent advances in neuroimaging analysis have demonstrated the utility of representing brain as simplicial complexes (Sizemore et al., 2018; Santoro et al., 2023), which preserves the inherent higher-order dependencies in neural systems that are critical for understanding cognitive processes and pathological mechanisms compared to two-way networks (Barrat et al., 2004). Based on this, we further propose the concept of monotonic weighted simplicial complex in Section 3.3 to explore some special higher-order structures in the brain and model neurobiological principles where functional coherence depends on hierarchical organization.

Specifically, for each temporal instance  $t$ , we can associate the  $k$ -order co-fluctuations with  $k$ -simplexes to construct four different monotonic weighted simplicial complexes. For example, the monotonic weighted simplicial complex  $\mathcal{K}_{positive,lower}^t$  that satisfies the lower closure condition and is linked with

positively synergistic interactions. The other three monotonic weighted simplicial complexes  $\mathcal{K}_{negative,lower}^t, \mathcal{K}_{positive,upper}^t, \mathcal{K}_{negative,upper}^t$  can be analogized from this. Specifically, in these simplicial complexes, a 0-simplex is a node associated with a ROI, a 1-simplex is a edge associated with pairwise interaction, a 2-simplex is a triangle associated with triplet interaction, a 3-simplex is a quadruplet associated with quadruplet interaction.

To construct these monotonic weighted simplicial complexes, we leverage the concept of filtration from Persistent Homology theory (Talesh Jafadideh and Mohammadzadeh Asl, 2022), a computational topology technique adept at analyzing high-dimensional datasets. Specifically, we design two types of filtrations to generate the monotonic weighted simplicial complexes that satisfies the lower closure condition, and the monotonic weighted simplicial complexes that satisfies the upper closure condition.

**The ascending filtration:** Sort the weights  $w^+$  in the set of all positively synergistic simplices  $S^+$  in ascending order and use the parameter  $\epsilon_l \in \mathbb{R}$  to scan this sequence  $S^+$ . At each step  $l$ , we include all 1-simplices, 2-simplices, and 3-simplices that satisfy the lower closure condition of the monotonic weighted simplicial complex to generate a monotonic weighted simplicial complex  $\mathcal{K}_{positive,lower}^t$ . The set of all negatively synergistic simplices  $S^-$  is processed in the same way to generate a monotonic weighted simplicial complex  $\mathcal{K}_{negative,lower}^t$ . These are defined as:

$$\begin{aligned} \mathcal{K}_{positive,lower}^t &= \{ \sigma \in S^+ \mid \text{for any face } \tau \text{ of } \sigma, w(\tau) \leq w(\sigma) \}, \\ \mathcal{K}_{negative,lower}^t &= \{ \sigma \in S^- \mid \text{for any face } \tau \text{ of } \sigma, w(\tau) \leq w(\sigma) \}. \end{aligned} \quad (8)$$

**The descending filtration:** Sort the weights  $w^+$  in the set of all positively synergistic simplices  $S^+$  in descending order and use the parameter  $\eta_l \in \mathbb{R}$  to scan this sequence  $S^+$ . At each step  $l$ , we include all 1-simplices, 2-simplices, and 3-simplices that satisfy the upper closure condition of the monotonic weighted simplicial complex to generate a monotonic weighted simplicial complexes  $\mathcal{K}_{positive,upper}^t$ . The set of all negatively synergistic simplices  $S^-$  is processed in the same way to generate a weighted simplicial complexes  $\mathcal{K}_{negative,upper}^t$ . These are defined as:

$$\begin{aligned} \mathcal{K}_{positive,upper}^t &= \{ \sigma \in S^+ \mid \text{for any face } \tau \text{ of } \sigma, w(\tau) \geq w(\sigma) \}, \\ \mathcal{K}_{negative,upper}^t &= \{ \sigma \in S^- \mid \text{for any face } \tau \text{ of } \sigma, w(\tau) \geq w(\sigma) \}. \end{aligned} \quad (9)$$

These weighted simplicial complexes encode the brain from different per-

spectives, providing the potential to further explore higher-order organizational patterns in the brain.

#### 4.3. Topological Lower-Order and Higher-Order Organizations of fMRI Signals

Many studies have explored higher-order structures in brain networks by focusing on loops (1D cycles) formed by nodes and edges (Bian et al., 2024; Bhattacharya et al., 2025), with limited attention paid to more complex higher-order organizational patterns. Besides, the influence of signed HOIs was overlooked in these studies, which could offer a broader diagnostic view of neurological conditions. The new definition of weighted simplicial complexes allows researchers to explore more complex signed higher-order structures, such as quadriplet structures and voids (2D holes) formed by triangular faces. This advance is significant because it further refines the HOIs by defining sign and links HOIs in the brain to higher-order organisations, and provides a higher-dimensional perspective for studying higher-order structures in the brain.

**Capture lower-order edges:** To explore brain activity patterns for diagnosis from a global perspective, we extract all the 1-simplices in the monotonic weighted simplicial complex  $\mathcal{K}_{positive,lower}^t$  and the monotonic weighted simplicial complex  $\mathcal{K}_{negative,lower}^t$  representing the lower-order organizations in brain and add them into a list  $\Delta^{edge} = \{(i, j), w_{ij}\}$ .

In this paper, we focus on the impact of signed HOIs, so we do not further explore the signs of lower-order edges. We construct a weighted matrix  $\tilde{A}^{edge} \in \mathbb{R}^{N \times N}$  from the list  $\Delta^{edge}$  and assign a weight  $w_{ij}$  equal to the weight of the edge for each element  $(i, j)$  in matrix.

**Capture higher-order good quadruplets:** To mine the topological higher-order of fMRI signals, we first extract all 3-simplices from the monotonic weighted simplicial complexes  $\mathcal{K}_{positive,lower}^t$  and  $\mathcal{K}_{negative,lower}^t$  and add them into two lists, respectively. These structures represent co-fluctuations that are not observable through lower-order interactions alone and represent extremely good higher-order organizations.

To quantify these good quadruplets at the edge levels from the lists, we use edge projections (Barrat et al., 2004). For each edge  $(i, j)$ , we assign a weight  $w_{ij}$  equal to the average sum of the weights of the quadruplets defined by that edge. The feature matrices of quadruplet signatures  $A^{lower} \in \mathbb{R}^{N \times N}$  using edge projections are illustrated in Figure 4.

**Capture higher-order 2D voids:** Similarly, we can extract all 3-simplices from the monotonic weighted simplicial complexes  $\mathcal{K}_{positive,upper}^t$  and  $\mathcal{K}_{negative,upper}^t$  to extract that represent extremely bad higher-order organizations. To some extent, these higher-order organizations can represent the 2-dimensional voids in the brain that are extracted by Persistent Homology, which reflect the intrinsic shape of the data from a higher-dimensional perspective. Therefore, we employ Persistent Homology (Talesh Jafadideh and Mohammadzadeh Asl, 2022) to extract 2-dimensional voids, which not only capture extremely bad higher-order organization but also help characterize the intrinsic geometric organization of neural activity from the perspective of a higher-dimensional manifold. More details about Persistent Homology theory and 2D void, please refer to Appendix A. The core concept involves constructing a filtration—a sequence of simplicial complexes  $\{S^l\}$  that progressively approximate the original weighted simplicial complex with increasing precision:

$$\emptyset = S^0 \subset S^1 \subset \dots \subset S^l \subset \dots \subset S^n. \quad (10)$$

Finally, the  $S^n$  is equal to the monotonic weighted simplicial complexes  $\mathcal{K}_{positive,upper}^t$  or  $\mathcal{K}_{negative,upper}^t$ . Persistent homology examines how higher-order topological features evolve through the filtration  $\{S^l\}$ , offering a measure of their robustness across scales. It is worth noting that calculating Persistent Homology requires defining the distance among multiple nodes in  $k$ -simplex, which can be easily achieved by computing  $1 - w_{i_0\dots i_k}$  (for  $k < 4$ ), where  $w_{i_0\dots i_k}$  represents the weight of the  $k$ -simplex.

By focusing on 2D voids within the homology group  $H_2$ , we track these higher-order organization. Specifically, we apply Persistent Homology to the monotonic weighted simplicial complexes  $\mathcal{K}_{positive,upper}^t$  and  $\mathcal{K}_{negative,upper}^t$  to generate two two-dimensional persistence diagrams. In each diagram, each point  $(b_g, d_g)$  signifies a void  $g$  that emerges during the filtration process. The persistence  $\pi_g = d_g - b_g$  quantifies the void’s lifespan, indicating its importance.

To better quantify the higher-order topological features captured by persistence homology, we employ a homological scaffold (Petri et al., 2014), a weighted network representing the topological features in the persistence diagram. This scaffold comprises all voids corresponding to generators  $g_i$ , weighted by their persistence  $\pi_{g_i}$ . Specifically, if an edge  $e$  belongs to multiple two-dimensional voids  $g_0, g_1, \dots, g_s$ , its weight  $\bar{w}_e^\pi$  is defined as the sum

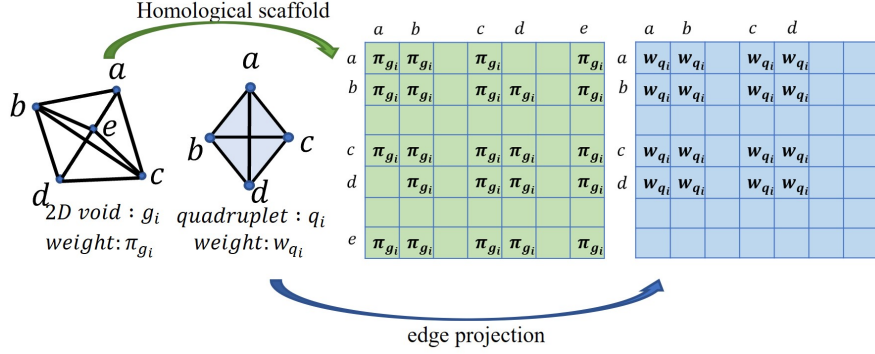


Figure 4: The illustration of the feature matrices of 2D voids using homological scaffold and the feature matrices of quadruplet signatures using edge projections.

of the persistences of these generators:

$$\bar{w}_e^\pi = \sum_{g_i | e \in g_i} \pi_{g_i}. \quad (11)$$

The homological scaffold reveals the roles of different links in shaping the system’s homological properties. A larger total persistence  $\bar{w}_e^\pi$  for a link  $e$  indicates its function as a locally strong bridge within the space of coherent and decoherent co-fluctuations. The feature matrices of 2D voids  $A^{upper} \in \mathbb{R}^{N \times N}$  using homological scaffold are illustrated in Figure 4.

At each time point  $t$ , five distinct weighted networks are constructed: one  $\tilde{A}^{edge}$  derived from edge structures representing lower-order interactions, two  $A_1^{lower}, A_2^{lower}$  from signed good quadruplet structures signifying HOIs, and another two  $A_1^{upper}, A_2^{upper}$  from signed 2D holes illustrating the data’s intrinsic geometric shape from a higher-dimensional perspective. By averaging across the entire time period, the resulting networks exhibit enhanced stability and mitigate the impact of fMRI noise.

#### 4.4. Multi-Channel Brain Network Transformer

To holistically integrate complementary information from heterogeneous topological features while preserving channel-specific properties, we propose a multi-channel brain network Transformer architecture with four coherently designed components.

#### 4.4.1. Signed Higher-Order Features Decoupling Mechanism

Higher-order features that are positive are related to patterns of simultaneous activation in multiple brain regions at a given moment, while higher-order features that are negative are related to patterns of collective inhibition in these regions at the current moment. These features can offer valuable information about complex coordination and communication within the brain. We further explore the influence of signed higher-order features using higher-order features decoupling mechanism. Specifically, for each type of higher-order feature, we consider two signed weighted matrices  $A_j^{lower}$  or  $A_j^{upper} \in \mathbb{R}^{N \times N}$  ( $j = 1, 2$ ). For each of these matrices, we extract its upper triangular part and flatten it to construct a feature vector  $h_j^{lower}$  or  $h_j^{upper} \in \mathbb{R}^{N(N-1)/2}$ . We generate two new higher-order topological features by adaptively learning weights to aggregate positive and negative information:

$$\alpha_1, \alpha_2 = \text{Softmax}(f^{lower}(h_1^{lower}, h_2^{lower})) \quad (12)$$

$$\tilde{A}^{lower} = \alpha_1 \odot A_1^{lower} + \alpha_2 \odot A_2^{lower} \quad (13)$$

$$\beta_1, \beta_2 = \text{Softmax}(f^{upper}(h_1^{upper}, h_2^{upper})) \quad (14)$$

$$\tilde{A}^{upper} = \beta_1 \odot A_1^{upper} + \beta_2 \odot A_2^{upper} \quad (15)$$

where  $f^{lower}$  and  $f^{upper}$  denote two separate two-layer multi-layer perceptrons (MLPs), and  $\tilde{A}^{lower}$  and  $\tilde{A}^{upper}$  denote, respectively, features of quadruplet structures and features of 2D voids that aggregate positive and negative information, respectively. The attention scores  $\alpha_i, \beta_i$  emphasize discriminative signed features while suppressing redundant signed information.

#### 4.4.2. Multi-Head Self-Attention Module of Multiple Channels

The feature matrices extracted above actually represent the low-order and higher-order topological information associated with each brain region separately. Simply feeding the concatenated low-order and higher-order information into the model would overlook the heterogeneity of the related information. Therefore, inspired by Brain network Transformer (Kan et al., 2022b), we leverage an  $L$ -layer non-linear mapping module, namely Multi-Head Self-Attention (MHSA), to generate more expressive node features using the low-order and higher-order topological features of multiple channels  $Z_i^L = \text{MHSA}(\tilde{A}_i) \in \mathbb{R}^{N \times N}$ , ( $i = 1, 2, 3$ ). Specifically, for each channel  $i$ , the output of each layer  $Z_i^l$  is obtained by

$$Z_i^l = (\|_{m=1}^M h_i^{l,m}\|) W_{O,i}^l \quad (16)$$

$$h_i^{l,m} = \text{Softmax} \left( \frac{\left( W_{Q,i}^{l,m} Z_i^{l-1} \right) \left( W_{K,i}^{l,m} Z_i^{l-1} \right)^\top}{\sqrt{d_{K,i}^{l,m}}} \right) W_{V,i}^{l,m} Z_i^{l-1} \quad (17)$$

where  $Z_i^{l=0} = \widetilde{A}_i$ ,  $\|\cdot\|$  is the concatenation operator,  $M$  is the number of heads,  $m$  is the head index,  $l$  is the layer index,  $W_O^l$ ,  $W_{Q,i}^{l,m}$ ,  $W_{K,i}^{l,m}$ ,  $W_{V,i}^{l,m}$  are learnable model parameters of each channel  $i$ , and  $d_{K,i}^{l,m}$  is the first dimension of  $W_{K,i}^{l,m}$ .

#### 4.4.3. Orthonormal Clustering Readout of Multiple Channels

Research has shown that low-level and high-level feature patterns in the brain often exhibit distinct functional modular structures, thereby supporting the richest functional interactions (Wang et al., 2019). Therefore, to leverage the inherent properties of brain networks, where nodes within the same functional module tend to exhibit similar behaviors and form clustered representations, we design an orthonormal clustering readout of multiple channels inspired by the reference (Kan et al., 2022b). This module is intended to capture modular-level similarities between ROIs across different brain network patterns, where nodes are softly assigned to well-defined clusters through an unsupervised process.

Formally, given  $K$  cluster centers where each center has  $V$  dimensions in a given channel  $i$ ,  $E_i \in \mathbb{R}^{K \times V}$ , a Softmax projection operator calculates the probability  $P_i^{jk}$  of assigning node  $j$  to cluster  $k$ :

$$P_i^{j,k} = \frac{e^{\langle Z_i^{L,j}, E_i^k \rangle}}{\sum_{k=1}^K e^{\langle Z_i^{L,j}, E_i^k \rangle}} \quad (18)$$

where  $\langle \cdot, \cdot \rangle$  denotes the inner product,  $k$  denotes the cluster index,  $Z_i^{L,j}$  is the learned embeddings of node  $j$  from the last  $L$ -th layer of the MHSA module in given channel  $i$ , and  $E_i^k$  denotes the embeddings of cluster  $k$  in given channel  $i$ . Using this soft assignment  $P_i \in \mathbb{R}^{N \times K}$  (where  $N$  is the number of nodes), the graph-level embedding  $Z_i^G$  is obtained by:

$$Z_i^G = P_i^\top Z_i^L. \quad (19)$$

To obtain representative soft assignment  $P_i$ , the initialization of cluster centers  $E_i$  is generated by orthonormal initialization (Kan et al., 2022b).

Table 1: Class distribution of brain network datasets.

Dataset	Class	# Subjects	Disease Type
ADNI	AD	90	Alzheimer’s Disease
	MCI	76	
	CN	96	
TaoWu	PD	20	Parkinson’s Disease
	NC	20	
PPMI	PD	53	Parkinson’s Disease
	prodromal	53	
ABIDE	ASD	488	Autism Spectrum Disorder
	NC	537	

#### 4.4.4. Attention-Guided Feature Fusion Mechanism for Classification

For embedding at the graph level  $F_i$  of each channel  $i$  obtained by flattening  $Z_i^G$  ( $i = 1, 2, 3$ ), we propose an attention-guided feature fusion mechanism to emphasize discriminative features while suppressing redundant information. The formula can be described as:

$$w_i = \sigma(q_i^T \tanh(W_i Z_i^G)) \quad (20)$$

$$\gamma_i = \frac{e^{w_i}}{e^{w_1} + e^{w_2} + e^{w_3}} \quad (21)$$

$$\tilde{F} = \gamma_1 \odot F_1 \parallel \gamma_2 \odot F_2 \parallel \gamma_3 \odot F_3 \quad (22)$$

where  $\sigma(\cdot)$  denotes sigmoid function,  $\odot$  is element-wise multiplication, and  $q_i^T$ ,  $W_i$  are learnable model parameters. Subsequently, a three-layer multi-layer perceptron (MLP) is employed using  $\tilde{F}$  as input for the prediction head. Finally, the cross-entropy loss function is used as the loss function.

## 5. Experiments

### 5.1. Experimental Settings

#### 5.1.1. Datasets and Preprocessing

To comprehensively evaluate the proposed method, we employ four fMRI datasets with varying sample sizes. The class distribution of brain network datasets is presented in Table 1. 1) **ADNI dataset** (Dadi et al., 2019): The Alzheimer’s Disease Neuroimaging Initiative (ADNI) primarily aims to investigate whether the combination of serial magnetic resonance imaging (MRI), positron emission tomography (PET), other biological markers, along

with clinical and neuropsychological assessments, can effectively measure the progression of mild cognitive impairment (MCI) and early Alzheimer’s disease (AD). The dataset comprises 90 Alzheimer’s disease (AD) patients, 96 cognitively normal (CN) subjects, and 76 individuals with mild cognitive impairment (MCI). 2) **TaoWu dataset** (Xu et al., 2023): Released by the International Conference on Imaging (ICI) (Xu et al., 2023), the TaoWu dataset represents one of the earliest neuroimaging collections for Parkinson’s disease research, containing 20 Parkinson’s disease (PD) patients and 20 normal controls (NC). 3) **PPMI dataset** (Xu et al., 2023): The Parkinson’s Progression Markers Initiative (PPMI) is a landmark longitudinal study designed to identify biomarkers of Parkinson’s disease risk, onset, and progression. Our study utilizes data from 53 Parkinson’s disease (PD) patients and 53 prodromal cases obtained from the PPMI database. 4) **ABIDE dataset** (Craddock et al., 2013): The Autism Brain Imaging Data Exchange (ABIDE) initiative facilitates Autism Spectrum Disorder (ASD) research by aggregating functional brain imaging data from multiple international sites. Our analysis includes 488 ASD patients and 537 normal controls (NC) from the ABIDE database.

All resting-state fMRI data were preprocessed following the pipeline described in (Esteban et al., 2019), which includes motion correction, realignment, field unwarping, normalization, bias field correction, and brain extraction. The preprocessed images were parcellated into 90 regions of interest (ROIs) using the Automated Anatomical Labeling (AAL) atlas (Tzourio-Mazoyer et al., 2002). The blood-oxygen-level-dependent (BOLD) time series for each ROI were obtained by averaging the time series of all constituent voxels.

### 5.1.2. Methods for Comparison

The selected baselines correspond to five categories. The first category consists of traditional machine learning models by the scikit-learn library (Pedregosa et al., 2011) using edge features, including Multilayer Perceptron (MLP), Support Vector Machine Classifier (SVM), Logistic Regression, and Random Forest. The second category consists of GNN-based models that learn lower-order topological features from a two-way network. These models include GCN (Kipf and Welling, 2017), GraphSAGE (Hamilton et al., 2017), GAT (Veličković et al., 2018), GroupINN (Yan et al., 2019), BrainGNN (Li et al., 2021), FBNetGen (Kan et al., 2022a), BPI-GNN (Zheng et al., 2024). The third category consists of Transformer-based models that utilize

the Transformer architecture to perceive the entire brain network, including Graph Transformer (Ying et al., 2021), Brain Network Transformer (Kan et al., 2022b), Tsen (Hu et al., 2023), Long-range Brain Transformer (Yu et al., 2024). The fourth category consists of higher-order methods based on hypergraph, including HGCN (Hao et al., 2023), HGAT (Wang et al., 2022). The fifth category consists of Persistent Homology (PH)-based models, including Brain-HORS (Santoro et al., 2024), PH-MCI (Bhattacharya et al., 2025), ATPGCN (Bian et al., 2024).

### 5.1.3. Implementation Details

For all experiments, we evaluated the performance in terms of diagnosis accuracy, recall, precision, and F1 score. For dataset partitioning, we adopt an 8:1:1 ratio for training, validation and testing for the ADNI dataset and ABIDE dataset, while using a 3:1:1 ratio for the TaoWu and PPMI datasets. When evaluating model performance, we implement 10-fold cross-validation for the ADNI dataset and ABIDE dataset while 5-fold cross-validation for the others. All models are trained using the Adam optimiser (Kingma and Ba, 2014) with an initial learning rate of  $10^{-4}$  and a weight decay of  $10^{-4}$ , in conjunction with the ReduceLRonPlateau scheduler (Paszke et al., 2017). The batch size is set to 16 for the ADNI dataset and ABIDE dataset while 4 for others, with a maximum number of epochs of 100. After each epoch, the model performance is evaluated using the validation set. We keep the model with the highest F1 score for testing. All experiments are run within the PyTorch framework (Paszke et al., 2017). Further implementation details are summarized below:

- In HOI-Brain, we employ a Julia-based implementation of the Ripserer and PersistenceDiagrams libraries (Bauer, 2021) to compute Persistent Homology and homological scaffold, extracting higher-order topological features.
- For traditional ML models, feature vectors were derived from the flattened upper triangle of Pearson correlation matrices computed from BOLD time series. An MLP with three fully connected layers is applied for classification. An SVM with a radial basis function kernel is applied for classification. A LogisticRegression with `solver=lbfgs` is applied for classification. A RandomForest with `n_estimators=300` is applied for classification.

- For GNN-based models and Transformer-based models, the correlation matrix is calculated using Pearson correlation for all time series. Node features are derived from the columns of the Pearson correlation matrix. The adjacency matrix in the graph is obtained by thresholding (0.5) the correlation matrix. Generally, two graph convolutional layers and an average pooling layer are used for classification.
- For hypergraph-based higher-order methods, specifically, for HGCN, a graph is first constructed through the correlation matrix, where the correlation of each edge of the graph is greater than 0.7. Each node constructs 2-hyperedges, 3-hyperedges, and 4-hyperedges by selecting its  $k$ -hop neighbors in the graph. For HGAT, the feature of the central node corresponding to each hyperedge is used as the hyperedge feature. During information aggregation, attention coefficients between hyperedges and nodes are computed for classification. Note that more HGNN-based methods applying to brain data have been proposed recently. However, the code of these models is not publicly available, and they require significant engineering which is difficult to reproduce faithfully based solely on the papers.
- For PH-based models (e.g., PH-MCI and ATPGCN), we use the persistent topological features of connected components  $H_0$  and loops  $H_1$  extracted by Ripsrer tool. For Brain-HORS, following the method, we extract the matrix of violating triangles, the matrix of one-dimensional loops and the matrix of lower-order edge features, which are then flattened and classified using an SVM.

The original codes shared by the authors of these baselines are used for the comparative analysis. We adapt their open-source codes, strictly follow the parameters provided in the papers, and modify them to fit our datasets.

## 5.2. Model Comparison

Tables 2–5 present the comparative results across the ADNI, TaoWu, PPMI, and ABIDE datasets. Performance metrics (mean  $\pm$  standard deviation) from ten-fold cross-validation are reported, with the best and second-best results highlighted in bold and underlined, respectively.

Several key observations emerge from our comparative analysis. First, general-purpose GNN-based models demonstrate comparable performance

Table 2: Performance comparison with five categories of baselines on the ADNI datasets(%). The best results are marked in bold and the second-best results in underlining.

Type	Method	Accuracy	Precision	Recall	F1-score
Traditional Machine Learning Models	MLP	66.3±5.8	67.4±6.4	68.3±6.4	69.1±5.8
	SVM	71.1±5.1	71.6±4.8	71.7±4.8	70.7±5.0
	Logistic Regression	70.7±5.9	73.3±7.7	71.7±7.1	70.5±7.2
	RandomForest	64.8±8.0	66.8±7.2	65.4±8.3	64.9±7.8
GNN-based models	GCN	60.9±11.8	61.6±12.5	61.1±11.9	60.3±12.1
	GraphSAGE	64.5±8.9	65.6±9.1	64.5±8.9	64.0±9.0
	GAT	60.0±10.1	61.8±10.6	60.0±10.1	59.2±10.3
	GroupINN	57.3±8.8	61.0±9.6	57.4±9.8	56.9±9.1
	FBNETGEN	66.4±7.0	67.7±7.5	67.4±7.1	60.8±5.9
	BPI-GNN	51.4±8.5	49.2±14.6	52.1±8.8	48.0±11.1
Transformer-based models	BrainGNN	58.9±7.7	60.5±8.8	58.9±7.7	58.2±8.0
	Graph Transformer	64.0±6.5	65.6±7.4	64.8±6.5	64.1±6.7
	BrainnetTransformer	69.6±6.2	72.2±6.2	69.5±6.8	69.2±6.3
	LR-BrainTransformer	<u>72.0±8.5</u>	<u>76.5±8.4</u>	<u>72.2±8.0</u>	<u>72.0±9.1</u>
HGNN-based models	TSEN	62.5±7.3	67.5±8.9	63.2±8.0	62.4±7.4
	HGCN	58.9±7.6	61.2±7.0	60.1±7.7	59.5±7.3
PH-based models	HGAT	54.5±7.5	55.4±7.7	55.3±6.7	54.7±6.9
	PH-MCI	64.8±6.9	67.8±7.3	64.3±5.7	63.5±6.2
	ATPGCN	70.8±6.7	72.6±7.3	70.6±6.3	70.8±6.7
Our Framework	Brain-HORS	64.0±7.2	66.2±7.0	64.0±7.2	64.1±6.8
	HOI-Brain	<b>75.9±8.6</b>	<b>80.0±7.9</b>	<b>75.6±9.1</b>	<b>75.5±9.2</b>

to traditional machine learning methods in most cases, without showing significant advantages. This can be attributed to neural networks’ increased parameter count when utilizing edge features, rendering them more prone to overfitting while maintaining better interpretability. Second, Transformer-based models consistently outperform GNN-based approaches across all four datasets, suggesting their superior capacity for capturing global connectome structures. Third, HGNN-based models show limited performance advantages, with notable results only on the PPMI dataset. We attribute this to: (1) their excessive parameterization increasing overfitting risk, and (2) their  $k$ -hop neighbor modeling failing to adequately represent co-fluctuation patterns among brain regions, thus poorly capturing HOIs. Notably, PH-based models (e.g., ATPGCN and Brain-HORS) demonstrate significant superiority over both GNN-based and traditional machine learning approaches by incorporating persistent homology-derived higher-order loop and connected component features. This underscores the critical importance of higher-order

Table 3: Performance comparison with five categories of baselines on the TaoWu datasets(%). The best results are marked in bold and the second-best results in underlining.

Type	Method	Accuracy	Precision	Recall	F1-score
Traditional Machine Learning Models	MLP	63.6±15.3	74.4±17.9	65.3±26.7	64.6±15.4
	SVM	57.5±12.8	65.0±22.6	40.0±20.0	46.8±17.1
	Logistic Regression	62.5±23.7	63.7±23.9	60.0±25.5	61.2±24.0
	RandomForest	67.5±16.0	71.3±17.3	70.0±18.7	67.9±11.1
GNN-based models	GCN	<u>72.5±18.4</u>	72.7±21.7	75.0±25.0	70.6±21.8
	GraphSAGE	67.5±20.3	68.3±21.3	60.0±25.5	63.6±23.5
	GAT	62.5±11.2	63.3±11.3	55.0±18.7	58.1±15.8
	GroupINN	62.5±7.9	59.7±19.0	62.5±7.9	58.5±13.3
	FBNETGEN	57.5±12.8	68.7±26.0	50.0±22.4	52.4±15.4
	BPI-GNN	55.0±12.8	56.7±15.8	55.0±12.8	53.7±12.7
	BrainGNN	60.0±16.6	57.7±19.5	57.6±22.3	60.0±16.6
Transformer-based models	Graph Transformer	67.5±6.1	<u>75.8±6.8</u>	67.5±6.1	64.6±8.1
	BrainnetTransformer	70.0±12.8	72.7±16.7	<b>80.0±24.5</b>	71.9±11.2
	LR-BrainTransformer	65.0±12.2	73.3±9.4	71.2±14.0	<u>74.0±12.1</u>
	TSEN	57.5±10.0	54.3±19.1	57.5±10.0	53.7±13.4
HGNN-based models	HGCN	55.0±20.3	58.7±23.1	55.0±20.3	52.4±20.2
	HGAT	57.5±15.0	59.0±17.4	57.5±15.0	56.3±15.3
PH-based models	PH-MCI	55.8±6.1	46.8±24.5	60.0±37.4	49.5±25.1
	ATPGCN	57.5±12.8	58.3±12.3	60.0±12.3	58.7±11.5
	Brain-HORS	57.5±20.3	58.3±21.1	57.5±20.3	57.2±20.2
Our Framework	HOI-Brain	<b>77.5±12.3</b>	<b>82.4±9.3</b>	<u>77.5±12.3</u>	<b>75.9±13.9</b>

topological features in brain disease diagnosis.

Our HOI-brain outperforms all 20 baselines on all datasets. In particular, it can be found that the proposed HOI-brain outperforms the traditional machine learning models on all datasets, with average accuracy improved by 12.5 (%), average precision improved by 12.9(%), average recall improved by 14.3(%) and F1-score improved by 12.7(%), respectively. And the proposed HOI-brain outperforms the GNN-based models on all datasets, with average accuracy improved by 19.6(%), average precision improved by 22.9(%), average recall improved by 19.5(%), and F1-score improved by 19.5(%), respectively. This indicates that our model, by incorporating higher-order topological features, is more beneficial for brain disease diagnosis compared to using only low-order edge features. Furthermore, the proposed HOI-Brain outperforms Transformer-based models on all datasets, with average accuracy improved by 13.0(%), average precision improved by 13.4(%), average recall improved by 10.3(%), and F1-score improved by 10.9(%), re-

Table 4: Performance comparison with five categories of baselines on the PPMI dataset (%). The best results are marked in bold and the second-best results in underlining.

Type	Method	Accuracy	Precision	Recall	F1-score
Traditional Machine Learning Models	MLP	61.3±5.3	<u>65.3±11.0</u>	54.5±11.4	58.1±6.4
	SVM	<u>64.2±8.3</u>	58.4±10.4	58.4±10.4	61.8±8.7
	Logistic Regression	60.5±7.0	62.4±7.2	54.7±16.8	56.8±11.0
	RandomForest	59.5±5.3	61.7±6.7	56.7±16.3	57.3±7.5
GNN-based models	GCN	57.5±6.8	58.7±10.1	62.4±5.1	59.6±3.7
	GraphSAGE	60.4±5.6	61.0±8.1	60.6±10.7	60.2±6.5
	GAT	61.3±6.8	61.3±7.3	64.4±8.1	60.4±6.3
	GroupINN	55.6±6.1	55.7±6.2	55.6±6.0	55.4±6.2
	FBNETGEN	59.4±8.4	60.6±10.9	62.4±5.1	60.8±5.9
	BPI-GNN	52.3±14.7	50.5±18.9	49.4±15.1	47.5±14.9
	BrainGNN	60.3±11.3	59.8±11.8	60.5±11.6	60.3±11.3
Transformer-based models	Graph Transformer	59.5±8.5	60.5±8.5	60.0±8.3	58.6±9.2
	BrainnetTransformer	60.4±7.4	65.1±15.9	58.6±15.4	59.1±7.8
	LR-BrainTransformer	58.6±7.0	59.8±10.7	64.4±8.5	60.9±4.7
	TSEN	58.5±7.6	59.3±7.9	58.6±7.5	57.8±7.6
HGNN-based models	HGCN	64.2±10.0	65.2±10.3	64.3±10.3	<u>63.4±10.5</u>
	HGAT	61.3±5.3	61.9±5.7	61.4±5.4	61.0±5.3
PH-based models	PH-MCI	53.6±4.1	58.8±6.5	60.0±8.4	55.5±6.6
	ATPGCN	61.2±3.5	62.1±3.4	<u>64.5±3.3</u>	62.9±3.3
	Brain-HORS	60.4±7.9	60.8±7.6	60.4±7.9	60.0±8.4
Our Framework	HOI-Brain	<b>66.1±4.0</b>	<b>69.0±4.0</b>	<b>66.3±4.2</b>	<b>64.7±4.7</b>

spectively. This highlights that our model, through the multi-channel brain network Transformer, can effectively and holistically integrate complementary information from heterogeneous higher-order and low-order topological features while preserving channel-specific properties. Next, when compared to HGNN-based models, HOI-Brain achieves remarkable improvements with average accuracy improved by 21.8(%), precision improved by 27.0(%), recall improved by 19.4(%), and F1-score improved by 20.5(%). These results clearly demonstrate that our proposed HOI-Brain framework significantly advances the modeling of HOIs through the Multiplication of Temporal Derivatives and the extraction of topological features using Persistent Homology in brain networks. When specifically compared to Persistent Homology (PH) based models, HOI-Brain achieves significant improvements with average accuracy increased by 17.4(%), precision enhanced by 21.4(%), recall boosted by 14.5(%), and F1-score elevated by 16.2(%). This is partly attributed to our method linking signed HOIs in the brain to higher-order organizations,

Table 5: Performance comparison with five categories of baselines on the ABIDE dataset (%). The best results are marked in bold and the second-best results in underlining.

Type	Method	Accuracy	Precision	Recall	F1-score
Traditional Machine Learning Models	MLP	58.3±6.3	60.3±5.0	59.6±5.4	58.7±6.4
	SVM	61.4±5.5	63.8±5.6	61.4±5.1	62.5±5.0
	Logistic Regression	63.1±5.9	65.5±5.9	63.1±5.3	64.2±5.3
	RandomForest	60.7±5.2	61.0±4.1	<b>68.3±8.4</b>	64.4±5.5
GNN-based models	GCN	60.4±4.5	61.8±4.3	64.4±7.5	62.9±4.7
	GraphSAGE	61.2±3.6	64.0±4.1	59.3±5.6	61.5±5.5
	GAT	59.3±3.8	57.9±5.3	61.1±3.5	59.5±4.8
	GroupINN	57.1±4.4	58.4±5.0	57.1±4.2	55.7±4.3
	FBNETGEN	58.0±4.2	59.8±4.1	61.1±8.6	60.1±5.2
	BPI-GNN	52.5±4.7	51.7±6.9	54.6±5.5	53.5±4.5
	BrainGNN	59.8±5.5	59.5±5.5	59.9±5.7	59.8±5.5
Transformer-based models	Graph Transformer	57.5±4.2	57.5±4.3	57.3±4.2	57.1±4.2
	BrainnetTransformer	63.1±5.8	64.6±5.8	<u>66.1±6.0</u>	<u>65.2±5.2</u>
	LR-BrainTransformer	<u>63.1±4.3</u>	<u>65.5±4.9</u>	63.3±6.0	64.2±4.3
	TSEN	60.5±4.6	59.3±3.9	59.1±5.1	59.8±3.6
HGNN-based models	HGCN	61.0±3.0	55.2±5.3	62.3±4.6	60.4±4.3
	HGAT	58.3±4.3	51.9±5.7	61.4±3.4	59.6±6.3
PH-based models	PH-MCI	57.9±5.2	58.4±4.6	61.5±4.5	59.3±6.2
	ATPGCN	62.2±4.5	62.4±5.3	60.6±5.3	61.8±4.6
	Brain-HORS	63.0±3.4	63.1±3.5	63.4±3.4	62.9±3.5
Our Framework	HOI-Brain	<b>65.6±3.5</b>	<b>66.2±3.8</b>	65.6±3.4	<b>65.3±3.5</b>

and partly due to our exploration of more complex signed quadruplet structures and 2D voids formed by triangular faces and quadruplet.

These experimental results demonstrate the effectiveness of our framework. To the best of our knowledge, our HOI-brain is the first method that distinguishes between positively and negatively synergistic HOIs, and the first attempt to utilize quadruplet-level interaction signatures and two-dimensional void descriptors extracted via Persistent Homology to enhance diagnostic efficacy.

### 5.3. Model analysis

#### 5.3.1. Ablation Study

To evaluate the rationality and effectiveness of the proposed model’s architecture, we conducted a series of ablation experiments to assess the impact of different components on overall performance. Our first aim was to evaluate the effectiveness of more complex signed quadriplet structures and 2D voids formed by triangular faces. Specifically, following the method in

Table 6: Performance comparison with varying combinations of features on the ADNI datasets (%). The best results are marked in bold and the second-best results in underlining.

Method	ADNI			
	Accuracy	Precision	Recall	F1-score
edge	68.4±5.5	69.9±5.4	69.3±6.0	68.1±5.7
edge+violating triangles+1D loops	59.7±7.5	61.8±9.5	60.6±7.6	59.0±7.9
edge+violating triangles+good quadruplets	73.9±7.8	74.6±7.2	73.8±8.0	73.7±7.8
edge+1D loops+2D voids	62.9±6.6	68.2±10.2	63.9±6.4	61.7±6.9
edge+good quadruplets+2D voids	<u>74.7±7.4</u>	<u>76.2±7.8</u>	<u>75.5±7.4</u>	<u>74.6±7.6</u>
edge+signed good quadruplets+signed 2D voids	<b>75.9±8.6</b>	<b>80.0±7.9</b>	<b>75.6±9.1</b>	<b>75.5±9.2</b>

Table 7: Performance comparison with varying combinations of features on the ABIDE datasets (%). The best results are marked in bold.

Method	ABIDE			
	Accuracy	Precision	Recall	F1-score
edge	58.3±5.3	58.3±5.4	59.1±4.1	58.1±5.5
edge+violating triangles+1D loops	61.6±4.4	60.0±4.2	63.5±5.9	62.4±4.1
edge+violating triangles+good quadruplets	60.5±4.2	62.4±4.7	59.4±4.3	61.7±4.3
edge+1D loops+2D voids	64.3±3.2	63.3±6.2	60.9±4.7	63.6±5.3
edge+good quadruplets+2D voids	<u>63.7±4.5</u>	<u>63.4±2.5</u>	<u>61.4±4.4</u>	<u>63.5±4.1</u>
edge+signed good quadruplets+signed 2D voids	<b>65.6±3.5</b>	<b>66.2±3.8</b>	<b>65.6±3.4</b>	<b>65.3±3.5</b>

(Santoro et al., 2024), we extracted lower-order edge features, violating triangles, and one-dimensional loops. In addition, we extracted unsigned good quadruplets and unsigned two-dimensional voids based on our methods. We implement it within different combinations of these features on all datasets. The experimental results presented in Tables 6, 7, B.8, B.9, indicate that integrating both higher-order and lower-order interactions proves to be more effective for brain disorder diagnosis compared to using lower-order interactions alone. Furthermore, quadruplet interactions captured by HOI-Brain have been demonstrated to be more effective in improving diagnosis than triplet interactions. This may be because a significant proportion of triplet interactions can be decomposed into a linear combination of pairwise interactions, which is insufficient to capture the true HOIs. Additionally, distinguishing between positively and negatively synergistic HOIs to generate signed higher-order structures, as opposed to unsigned ones, can further improve the effectiveness of brain disease diagnosis, which may be due to the fact that it can provide detailed insights into the communication within the

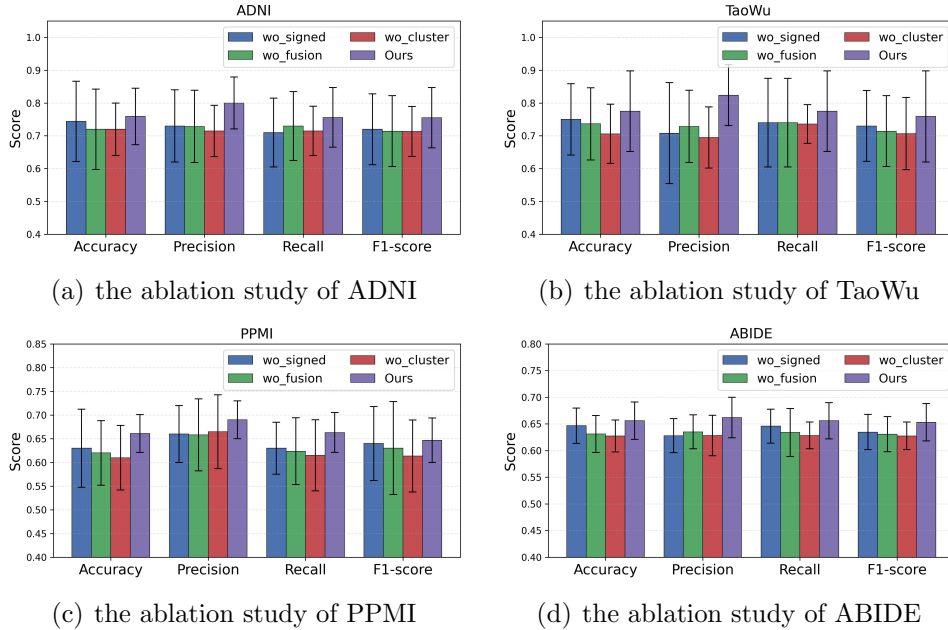


Figure 5: Results of the ablation study in in multi-channel brain network Transformer of HOI-Brain, comparing with three degenerated variants for all datasets.

brain.

Our second aim was to evaluate the effectiveness of different components in multi-channel brain network Transformer. The different variants are: not adding signed higher-order features decoupling mechanism (wo-signed), not adding attention-guided feature fusion mechanism (wo-fusion), and not adding orthonormal clustering readout of multiple channels(wo-cluster). From Figure 5, we can see that adding signed higher-order features decoupling mechanism and attention-guided feature fusion mechanism are always helpful as HOI-brain outperforms all variants, including (wo-signed) and (wo-fusion). This result is consistent with our assumption that by introducing the attention mechanism, our model can adaptively fuse both positive/negative information and multi-channel information, thereby emphasizing discriminative features while suppressing redundant information. Incorporating orthonormal clustering readout across multiple channels (wo-cluster) is highly beneficial, as this approach effectively captures both lower-order and higher-order feature patterns, which often reside within distinct functional modular structures.

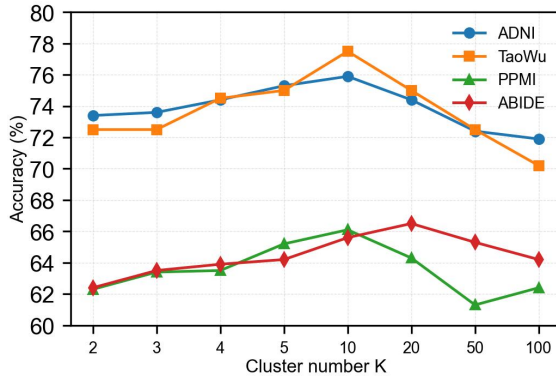


Figure 6: Influence of the key hyper-parameter, the number of clusters, for model performance on accuracy metrics.

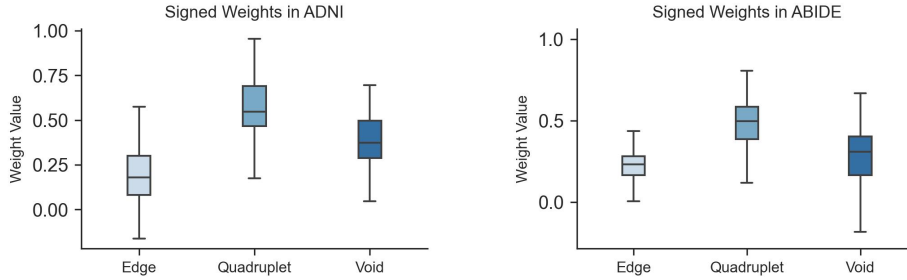
### 5.3.2. Hyperparameter Analysis

To further demonstrate how the design of orthonormal clustering readout across multiple channels affects our model’s performance, we investigate a key hyperparameter: the number of clusters  $K$ . Specifically, we evaluate the method with  $K$  set to 2, 3, 4, 5, 10, 20, 50, and 100. The accuracy metric results when tuning this hyperparameter across all datasets are presented in Figure 6. The results of other metrics are presented in Figure C.19. We observe that the model’s performance improves as  $K$  increases from 2 to 10 or 20 but declines when  $K$  rises from 10 or 20 to 100. This suggests that the optimal number of clusters is relatively small, reducing computational cost while aligning with the fact that the typical number of functional modules is fewer than 25, a finding consistent with previous studies (Kan et al., 2022b).

## 5.4. Model Interpretability

### 5.4.1. In-depth Analysis of Attention Mechanism

To better understand the mechanism of our model, which focuses on the most discriminative information in the brain for the diagnosis of brain diseases, we first performed a visualization analysis of the attention scores  $\gamma_1, \gamma_2$  of the attention-guided feature fusion mechanism for all patients of each type of disease, using ADNI and ABIDE as examples. Figure 7 shows that our model is capable of adaptively learning weights according to the characteristics of different diseases, thereby integrating higher-order and lower-order topological information for the diagnosis of brain diseases. In addition, we



(a) the attention scores of each channel in ADNI (b) the attention scores of each channel in ABIDE

Figure 7: The visualization of attention scores for each channel in (a) the ADNI dataset and (b) the ABIDE dataset, as two examples.

observed that quadruplet-level interaction signatures are significantly more important than two-dimensional void descriptors and edge features, with their average attention scores exceeding 0.5 on both datasets.

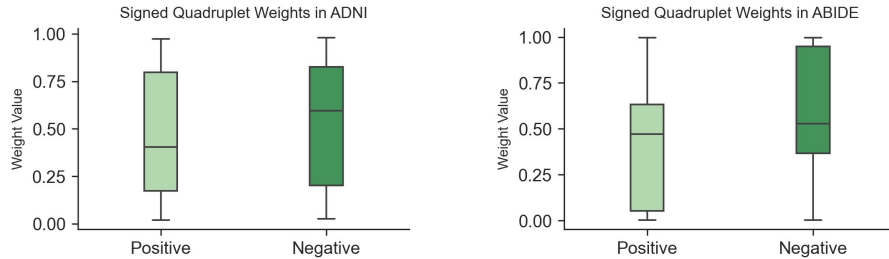
Next, we also conducted a visualization analysis of the attention scores  $\alpha_1, \alpha_2, \beta_1, \beta_2$  derived from the signed higher-order feature decoupling mechanism for all patients across each disease type, using ADNI and ABIDE as examples. Figure 8 shows that across both datasets, the importance of negatively synergistic quadruplets is generally greater than that of positively synergistic information in most cases, while the importance of positively synergistic voids exceeds that of negatively synergistic information. This new phenomenon may provide a clearer direction for research into the pathological mechanisms of brain diseases.

In order to conduct a more in-depth investigation into the aforementioned phenomena in the attention mechanism, inter-group comparisons were conducted of the signed higher-order topological features, the quadruplet-level interaction signatures and two-dimensional void descriptors. These were captured by the model in both the patient and healthy control groups. The ADNI dataset was used as an example. As demonstrated in Figure 9, which presents a comparison of group differences in the number of higher-order topological features, it was observed that the group differences in the quadruplet-level interaction signatures were found to be highly significant, with all statistical significance levels at  $p < 0.001$  compared to void descriptors. This finding is consistent with the results of our model visualisation. This phenomenon may be attributed to the disruption of HOIs within the

brain during the progression of the disease, which in turn exerts an influence on the high-dimensional hole structures present within the brain. Furthermore, as the disease progresses, the number of positive quadruplets exhibits a gradual decrease, while the number of negative quadruplets initially decreases and subsequently increases. This finding suggests that during the transition from CN to MCI, there is a decline in synergistic interactions in the brain, whether positive or negative, as brain communication becomes progressively disrupted. Conversely, as the condition progresses from MCI to AD, brain regions have been observed to exhibit more negatively synergistic interactions, concurrently reducing their excitability to preserve the functionality of diverse neural modules. This finding aligns with the reference stating that excitatory neurons in the brains of Alzheimer’s patients suffer severe genomic damage (Miller et al., 2022). With regard to the number of voids, although no clear trend was observed in the progression of the disease, it was found that positive voids exhibited more significant inter-group differences compared to negative voids. This finding lends further support to the hypothesis that they exhibit higher levels of attention scores. Consequently, CN appears to utilise positive information to construct the whole-brain topological structure, whereas AD relies more heavily on negative information. These findings may offer a novel perspective on the pathological mechanisms underlying Alzheimer’s disease.

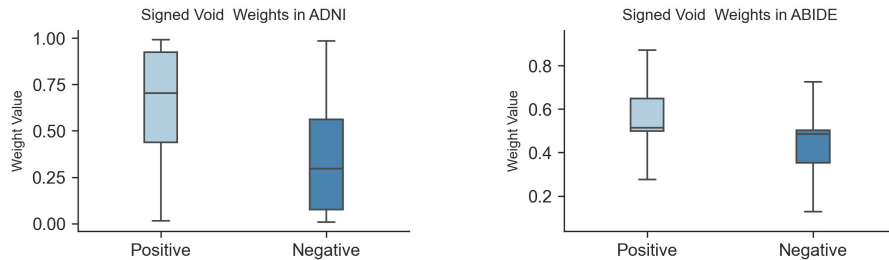
#### 5.4.2. *In-depth Analysis of Cluster Mechanism*

To better understand how our model leverages modular-level similarities between ROIs across different brain network patterns, we first provide a visualization of three attention matrices at the first layer of the multi-head self-attention module on the ADNI and ABIDE datasets in Figures 10, 11. The attention scores are averaged across all subjects in the ADNI or ABIDE test set. This figure demonstrates that the learned attention scores reveal varying degrees of modularity in both lower-order and higher-order patterns, highlighting the interpretability of our model. Furthermore, we provide a visualization of three cluster assignment matrices on the ADNI or ABIDE dataset in Figure 12. The cluster assignment matrices are multiplied across layers and averaged across all subjects in the ADNI and ABIDE test set. Each row corresponds to an ROI and each column is a cluster. We observe that the assignment matrix, which is calculated based on the similarity between nodes and clusters, contains only one high-value entry per row in most cases, despite the fact that we did not impose any regularization constraints



(a) the attention scores of quadruplet in ADNI

(b) the attention scores of quadruplet in ABIDE



(c) the attention scores of void in ADNI

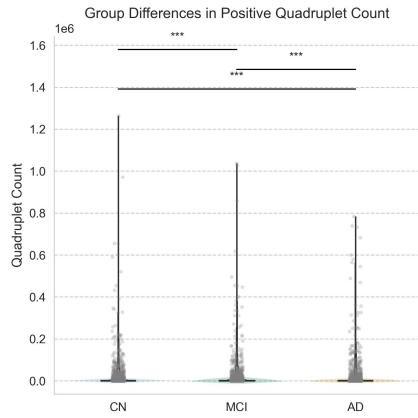
(d) the attention scores of void in ABIDE

Figure 8: The visualization of attention scores for quadruplet in (a) the ADNI dataset and (b) the ABIDE dataset, and the visualization of attention scores for void in (c) the ADNI dataset and (d) the ABIDE dataset.

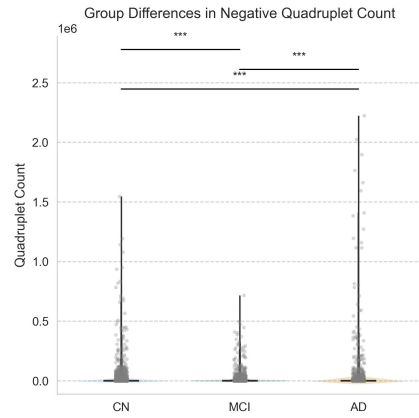
on the assignment matrix. This indicates that our model can effectively partition nodes into functional modules. Additionally, there are differences between the assignment matrices of low-order and higher-order patterns, which further demonstrates that varying degrees of modularity in both low-order and higher-order patterns. This result aligns with the visualization of three attention matrices, further indicating the interpretability of our model.

### 5.4.3. The Important Brain Regions and Interactions of Brain Regions

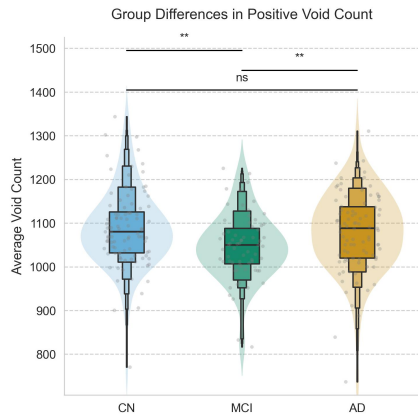
In this section, we further investigate whether the learned ROIs attention scores are interpretable and consistent with previous findings. Here, we take the ADNI, PPMI and ABIDE datasets as examples for discussion of three diseases. These three datasets contain larger sample sizes, enabling the reflection of more generalizable phenomena for brain diseases. First, we analyze the important brain regions and interactions of brain regions associated



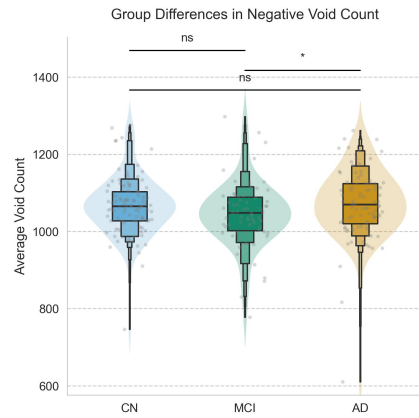
(a) the number of positive quadruplets



(b) the number of negative quadruplets



(c) the number of positive voids



(d) the number of negative voids

Figure 9: Group difference comparison of the signed higher-order topological feature quadruplet-level interaction signatures and two-dimensional void descriptors on ADNI. Statistical significance is denoted as follows: \*\*\* $p < 0.001$ , \*\* $p < 0.01$ , \* $p < 0.05$ , and ns  $p \geq 0.05$ .”

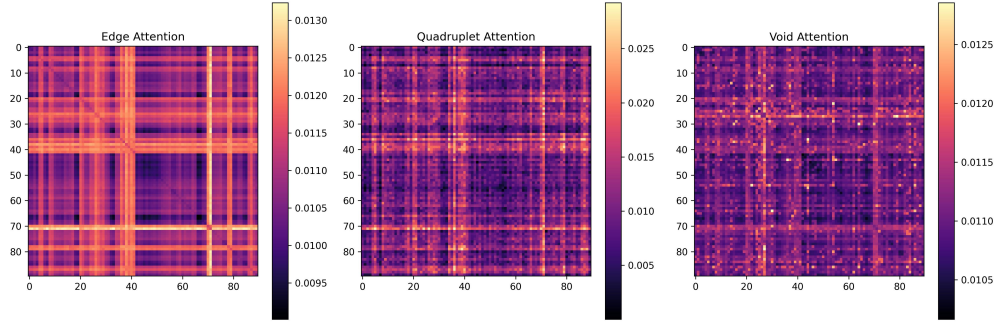


Figure 10: Visualization of three attention matrices at the first layer of multi-head self-attention module on ADNI.

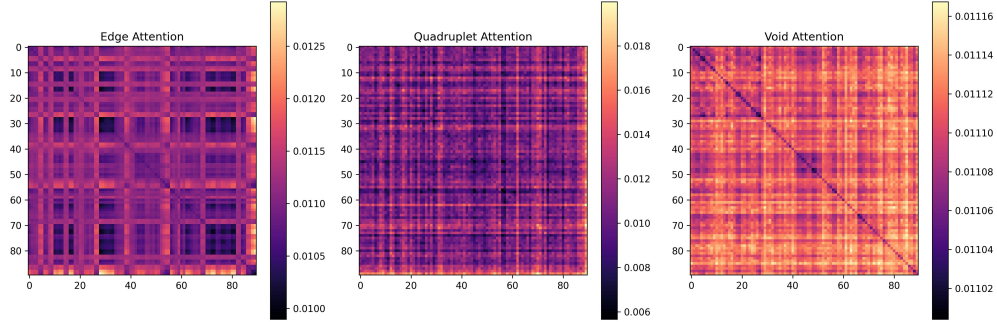
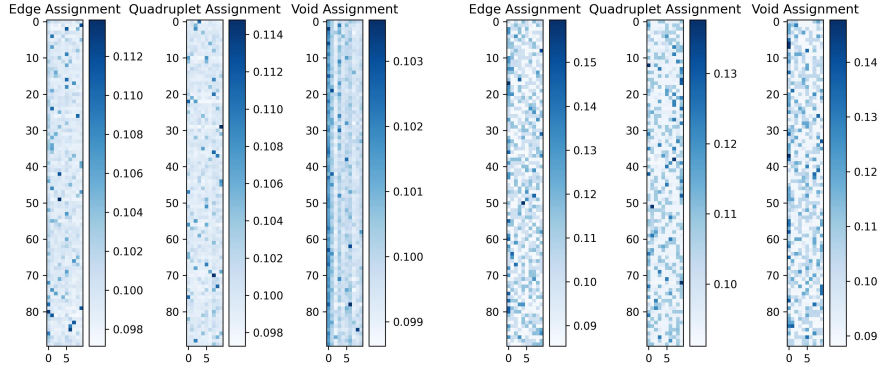


Figure 11: Visualization of three attention matrices at the first layer of multi-head self-attention module on ABIDE.

with brain diseases using HOI-Brain from a more comprehensive perspective rather than a low-level perspective as in previous studies (Kan et al., 2022b; Yu et al., 2024). For each subject, HOI-brain generates three attention matrices at the first layer of multi-head self attention module. Higher attention scores indicate greater discriminative power of the regions for AD, PD, and ASD. For each disease, we obtain a comprehensive attention matrix that simultaneously captures both lower-order and higher-order patterns by performing a weighted summation of the three attention matrices for each individual, with the weights derived from the attention scores of each channel. At the regional and regional interaction level, we average the integrated attention matrices across all individuals to construct a matrix representing the importance of interactions between regions. At the regional level, we further compute the row-wise mean of this matrix to obtain the final regional importance scores. We visualize the top ten ROIs and interactions of ROIs



(a) three cluster assignment matrices on ADNI. (b) three cluster assignment matrices on ABIDE.

Figure 12: Visualization of three cluster assignment matrices on ADNI and ABIDE datasets.

with the highest attention scores using BrainNet Viewer (Xia et al., 2013), respectively.

**Alzheimer’s disease (AD).** From the Figure 13, we observed a significant overlap between the ROIs and those implicated in critical interactions, particularly involving the left caudate nucleus. This may be attributed to the damage sustained by relevant brain regions during the progression of Alzheimer’s disease, which subsequently leads to weakened connectivity between brain regions. The ten ROIs with the highest attention scores include: Right Caudate (CAU.R), Left Hippocampus (HIP.L), Right Parahippocampal Gyrus (PHG.R), Left Amygdala (AMYG.L), Left Olfactory Cortex (OLF.L), Left Middle Temporal Gyrus (TPOmid.L), Right Olfactory Cortex (OLF.R), Left Parahippocampal Gyrus (PHG.L), Left Caudate (CAU.L), and Right Heschl’s Gyrus (HES.R). These regions are primarily associated with functions such as memory (Hippocampus, Parahippocampal gyrus), emotion (Amygdala), olfaction (Olfactory cortex), motor control (Caudate nucleus), and auditory processing (Heschl’s gyrus). Specifically, the Hippocampus and Parahippocampal gyrus have been widely confirmed to be associated with AD (Bv and Agrawal, 2022; Echávarri et al., 2010), as they are involved in brain memory functions. The Amygdala has also been widely demonstrated to undergo atrophy during the progression of diseases (Zidan et al., 2019). The Caudate, due to its crucial role in regulating motor control, has significant associations with AD (Zhi et al., 2024). Ye et al. also

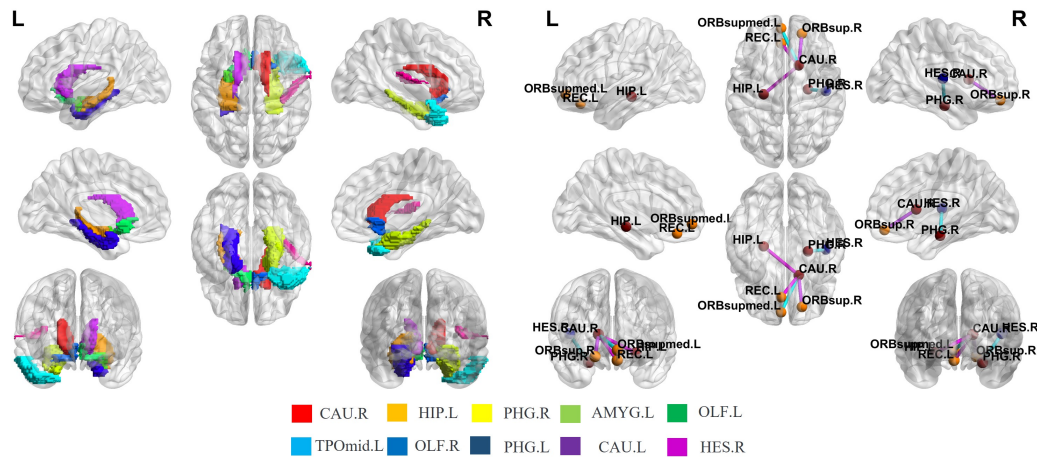


Figure 13: Visualization of top 10 important brain regions(left) and top 10 important interactions of brain regions(right) associated with ADNI.

confirmed the association between the Middle Temporal Gyrus and AD (Ye et al., 2019). The Olfactory Cortex and the Heschl’s Gyrus currently lack direct evidence linking them to Alzheimer’s disease. However, they may be associated with the decline of hearing and smell in Alzheimer’s patients, which suggests that this finding obtained by HOI-brain may provide new insights into the pathology of Alzheimer’s disease. In addition, we observed that most of the top ten ROI interactions with the highest attention scores revolve around the Right Caudate, suggesting that the Right Caudate may serve as a hub node in the brain network and is disrupted during the progression of Alzheimer’s disease, which is consistent with the literature (Zhi et al., 2024).

**Parkinson’s disease (PD).** As illustrated in Figure 14, the ten ROIs with the highest attention scores are: Right Precentral Gyrus (PCG.R), Left Medial Orbitofrontal Cortex (ORBsupmed.L), Right Inferior Parietal Lobule (IPL.R), Left Amygdala (AMYG.L), Right Triangular Part of the Inferior Frontal Gyrus (IFGtriang.R), Right Superior Parietal Gyrus (SPG.R), Right Inferior Orbitofrontal Cortex (ORBinf.R), Right Thalamus (THA.R), Right Superior Temporal Gyrus (STG.R), and Right Opercular Part of the Inferior Frontal Gyrus (IFGoperc.R). These regions are predominantly implicated in motor execution, reward processing, executive control, affective regulation, and sensorimotor integration—domains known to be disrupted in PD. Specifically, the Precentral Gyrus, a key component of the primary motor

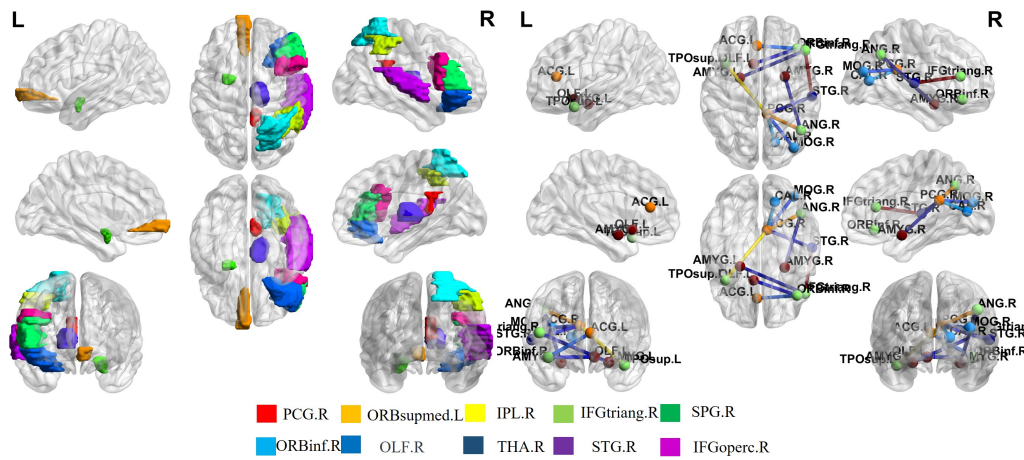


Figure 14: Visualization of top 10 important brain regions(left) and top 10 important interactions of brain regions(right) associated with PPMI.

cortex, exhibits marked hypometabolism and altered functional connectivity in PD (Wang et al., 2024b). The left medial orbitofrontal cortex is related to decision-making performance in Parkinson’s disease (Kobayakawa et al., 2016). Moreover, compared with normal controls, patients with PD showed a globally reduced structural-functional connectivity decoupling in the Inferior and Medial Orbitofrontal Cortices (ORBinf.R and ORBsupmed.L) (Zou et al., 2024). The Amygdala, central to emotional processing and reward evaluation, demonstrates reduced volume and disrupted connectivity within limbic-striatal circuits in PD, which may underlie affective dysregulation and apathy (Yoshimura et al., 2005). The Thalamus, a vital relay hub within cortico-basal ganglia-thalamo-cortical loops, is frequently implicated in PD pathophysiology due to its role in motor and non-motor symptomatology, including tremor and cognitive fluctuations (Zirh et al., 1998). The Triangular and Opercular parts of the Inferior Frontal Gyrus (IFGtriang.R and IFGoperc.R), critical for executive control and language processing, demonstrate impaired activation and connectivity in PD, aligning with cognitive inflexibility and verbal fluency deficits (Li et al., 2020). It is worth noting that although there is currently no direct literature indicating a pathological association between the superior temporal gyrus and PD, its involvement in auditory processing and social cognition may indirectly contribute to communication difficulties and social withdrawal symptoms in patients with Parkinson’s disease. Importantly, unlike ADNI and ASD, the core hubs in the interac-

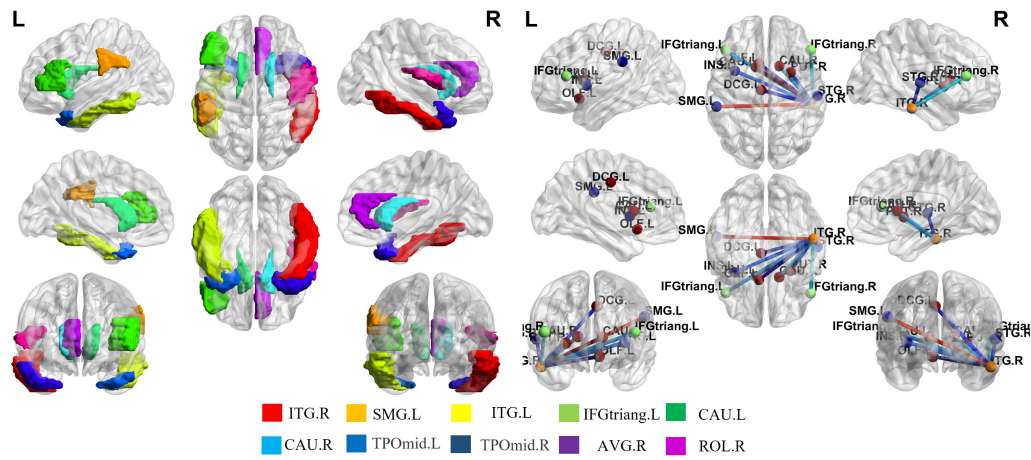


Figure 15: Visualization of top 10 important brain regions(left) and top 10 important interactions of brain regions(right) associated with ABIDE.

tion network—PCG.R, STG.R, IFGtriang.R, and ANG.R—were not among the most highly ranked regions in terms of brain importance. Conversely, the seven brain regions identified as key in terms of importance—such as ACG.R, TPOmid.R, and CAU.L—were almost entirely absent from the top 20 regions with the strongest interactions. Together, these findings underscore two distinct interpretations of importance in the brain: global centrality versus local strong coupling.

**Autism Spectrum Disorder (ASD).** As illustrated in Figure 15, the ten ROIs with the highest attention scores are: Right Inferior Temporal Gyrus (ITG.R), Left Supramarginal Gyrus (SMG.L), Left Inferior Temporal Gyrus (ITG.L), Left Triangular Part of the Inferior Frontal Gyrus (IFGtriang.L), Left Caudate (CAU.L), Right Caudate (CAU.R), Left Middle Temporal Gyrus (TPOmid.L), Right Middle Temporal Gyrus (TPOmid.R), Right Anterior Cingulate Gyrus (ACG.R), and Right Rolandic Operculum (ROL.R). These regions are predominantly implicated in social cognition, language processing, executive control, and sensorimotor integration. Specifically, the Inferior Temporal Gyrus has been repeatedly reported to exhibit atypical activation and connectivity patterns in individuals with ASD, reflecting its crucial role in face perception and semantic processing (Kim et al., 2021). The Supramarginal Gyrus, a core component of the mirror-neuron system, has also been shown to demonstrate aberrant functional connectivity in ASD, which may contribute to deficits in empathy and social interaction (Bi

et al., 2025). The Caudate nucleus, given its involvement in reward processing and cognitive flexibility, has been associated with restricted and repetitive behaviors characteristic of ASD (Adorjan et al., 2017). Furthermore, the Middle Temporal Gyrus and the Anterior Cingulate Gyrus have been implicated in the pathophysiology of ASD through their roles in theory-of-mind and conflict monitoring, respectively (Zhu et al., 2022; Xu et al., 2019). The Rolandic Operculum, although less frequently discussed, is closely linked to auditory and sensorimotor integration, the disruption of which may underlie sensory hypersensitivity commonly observed in ASD (Zhang et al., 2025). Notably, the majority of the top ten ROI interactions with the highest attention scores center on ITG.R, suggesting that this region may also function as a pivotal hub within the brain network and is selectively disrupted during the progression of ASD. This finding aligns with recent literature highlighting the central role of the ITG in the neurodevelopmental trajectory of autism (Kim et al., 2021).

#### *5.4.4. The Higher-Order Organizations that Differ between Patients and Healthy Individuals*

Next, we further investigate whether the HOIs among key brain regions identified by HOI-Brain show significant differences during disease progression, which could offer additional therapeutic insights for brain disease research. For ease of calculation, we selected four out of the top ten key brain regions identified for each disease. Using our proposed Multiplication of Temporal Derivatives (MTD)-based co-fluctuation calculation method, we computed the quadruplet interactions among the relevant brain regions and subsequently compared the group differences. As shown in Figures 16, 17, 18, compared to other brain regions, although these brain regions all demonstrate significant importance in the diagnosis of AD or ASD—indicating that they may have sustained varying degrees of damage—their HOIs exhibit notable differences across various stages of disease progression. This suggests a dissociation between HOIs in the brain and the functions of the individual brain regions themselves, which is consistent with the literature (Wang et al., 2019). In addition, we observed that during the transition from healthy individuals to those with AD or ASD, the positive HOIs between relevant brain regions gradually weaken, indicating a progressive impairment of higher-order synergistic functions among brain regions. On the other hand, the negative HOIs between these brain regions gradually strengthen, reflecting an increasing degree of internal functional disruption in the brain. This phenomenon is

consistent with findings reported in previous literature (Santoro et al., 2024). However, this phenomenon is exactly the opposite in PD, which may be due to the fact that Parkinson’s patients, because of their motor impairments, are prone to hallucinations. Hallucinations in Parkinson’s disease may result from excessive influence of higher-order brain regions on early sensory processing, which is consistent with the enhanced functional integration between sensory and higher-order networks (Tan et al., 2023).

**Alzheimer’s disease (AD).** As shown in Figure 16, in particular, the quadruplet interaction among CAU.R, HIP.L, PHG.R, and AMYG.L; the quadruplet interaction among OLF.L, HIP.L, PHG.R, and AMYG.L; and the quadruplet interaction among CAU.R, OLF.L, PHG.R, and AMYG.L, which involve the cortico-striatal-olfactory circuit, exhibit significant inter-group differences during the progression from CN to MCI, with  $p$ -values  $< 0.05$ . However, these differences become less pronounced during the progression from MCI to AD, with  $p$ -values  $\geq 0.05$ . This suggests that these HOIs may serve as potential biomarkers for the early diagnosis of Alzheimer’s disease. In contrast, the quadruplet interaction among CAU.R, TPOmid.L, HIP.L, and AMYG.L, which involves the social-reward-emotion-memory integrated circuit, shows significant inter-group differences throughout the entire AD progression, with  $p$ -values  $< 0.001$ . This indicates that these HOIs may be persistently disrupted across the entire disease course, playing a critical role in AD pathogenesis.

**Parkinson’s disease (PD).** As shown in Figure 17, the quadruplet interaction among PCG.R, ORBsupmed.L, IPL.R, and SPG.R; the interaction among PCG.R, ORBsupmed.L, IPL.R, and IFGoperc.R; and those among PCG.R, ORBsupmed.L, IPL.R, and STG.R, which collectively engage the dorsal attention network and fronto-parietal executive control circuits, exhibit significant inter-group differences ( $p < 0.05$ ) between prpdromal and PD. These findings suggest that these functional connectivity patterns may serve as potential early biomarkers for cognitive-motor integration deficits characteristic of the prodromal stages of PD. In addition, the quadruplet interaction involving PCG.R, ORBsupmed.L, THA.R, and IFGoperc.R, which maps onto the mesocortical limbic-striatal-thalamic loop, shows inter-group differences ( $p < 0.001$ ). This persistent disruption aligns with the progressive degeneration of dopaminergic pathways and thalamocortical relay integrity, implicating these interactions in both motor dysfunction (e.g., bradykinesia) and nonmotor symptoms (e.g., apathy, executive dysfunction) throughout the pathogenesis of PD-related motor and cognitive impairment.

**Autism Spectrum Disorder (ASD).** From Figure 18, we observed that the quadruplet interactions among the key brain regions—including the interactions among ITG.R, SMG.L, ITG.L, and IFGtriang.L; among SMG.L, ITG.L, IFGtriang.L, and CAU.L; among ITG.R, ITG.L, IFGtriang.L, and CAU.L; among ITG.R, SMG.L, IFGtriang.L, and CAU.L; and among ITG.R, SMG.L, ITG.L, and CAU.L, which involves a visual-auditory-semantic-action-control closed-loop system. These interactions exhibited significant inter-group differences throughout the entire progression of ASD. Such quadruplet interactions may serve as potential biomarkers for investigating tool-use deficits, semantic control impairments, and action-language disconnection in social communication associated with autism. However, the quadruplet interaction among ITG.L, IFGtriang.L, CAU.L, and CAU.R shows no significant inter-group differences throughout the entire AD progression, with p-values  $\geq 0.05$ . This suggests a dissociation between higher-order brain interactions and the functions of individual brain regions themselves.

## 6. Discussion

### 6.1. The model

Recent conceptual and technical advances in fMRI data analysis provide an opportunity for the field to not only improve the effectiveness of brain disease diagnosis but also deepen our understanding of brain disease mechanisms (Zheng et al., 2024; Luo et al., 2025; Kan et al., 2022b; Yu et al., 2024; Wang et al., 2022; Hao et al., 2023; Bian et al., 2024; Bhattacharya et al., 2025). However, current methods overlook more higher-order patterns with signs, limiting an integrated understanding of brain-wide communication for brain disease diagnosis.

In this study, we focused on the importance of signed higher-order (group) interactions in fMRI signals, which were inferred using a recently developed topological approach (Hyekyoung et al., 2011). Our proposed HOI-Brain incorporates: (i) a novel higher-order interaction representation strategy via Multiplication of Temporal Derivatives (MTD) to quantify dynamic functional co-fluctuations of group ROIs; (ii) a new definition of weighted simplicial complex is proposed and a novel higher-order feature extraction method is employed on them focusing on quadruplet-level interaction signatures and two-dimensional void descriptors through Persistent Homology; (iii) a pioneering effort to distinguish between positively and negatively synergistic higher-order interactions in the brain; (iv) a novel multi-channel brain

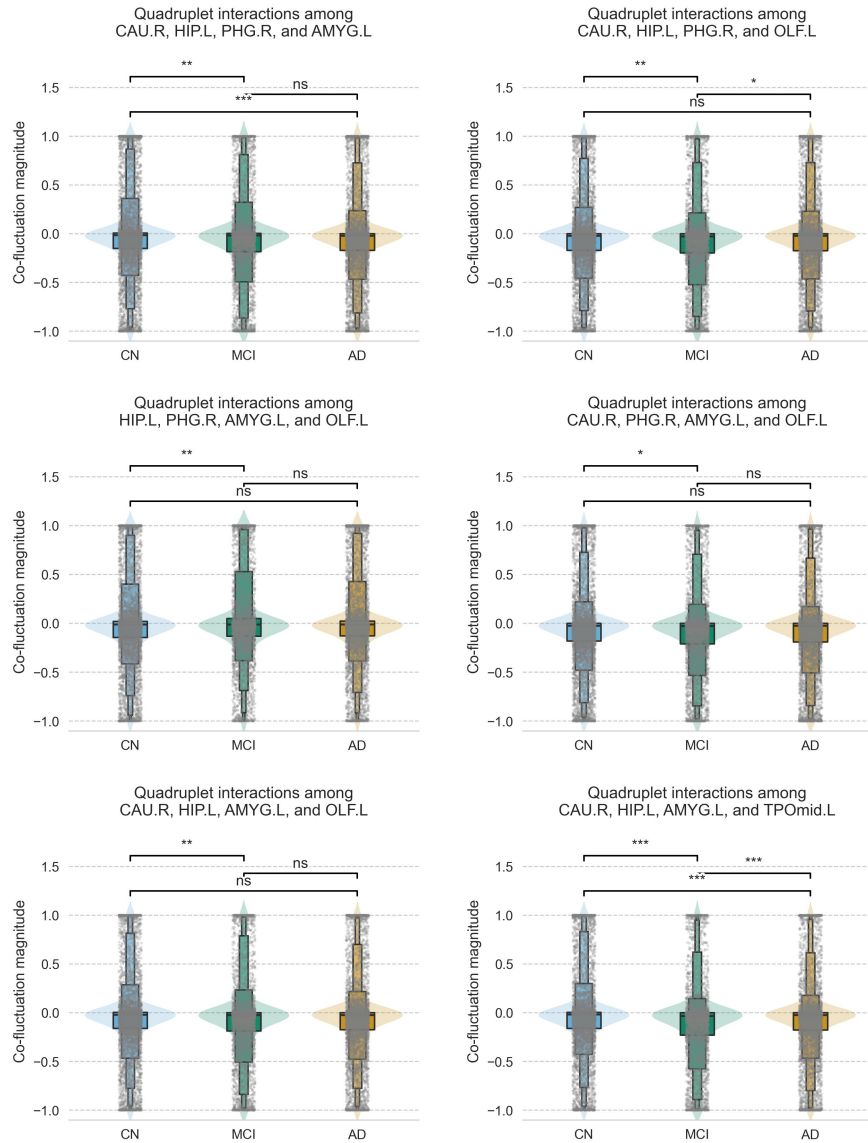


Figure 16: Group difference comparison of quadruplet interactions among the relevant brain regions (CAU.R, HIP.L, PHG.R, AMYG.L, OLF.L, TPOmid.L) on ADNI. Statistical significance is denoted as follows: \*\*\* $p < 0.001$ , \*\* $p < 0.01$ , \* $p < 0.05$ , and ns  $p \geq 0.05$ .”

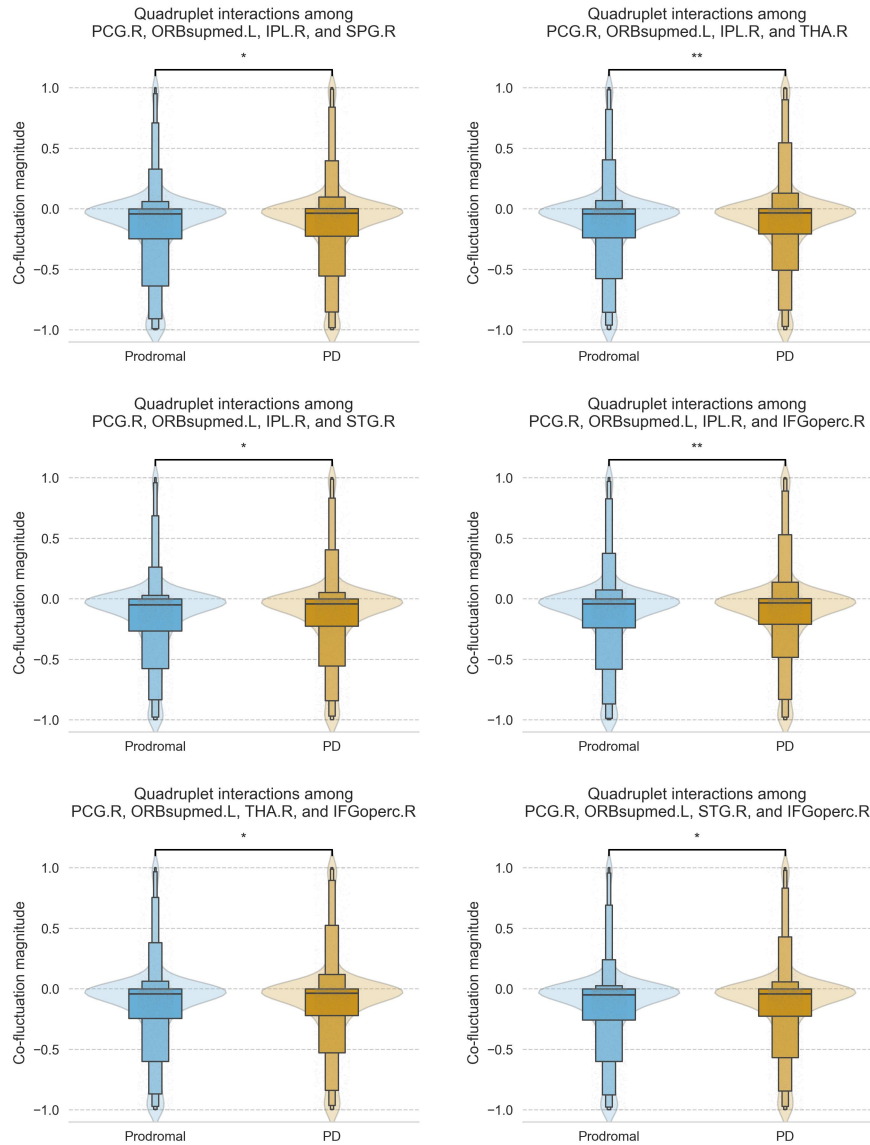


Figure 17: Group difference comparison of quadruplet interactions among the relevant brain regions (PCG.R, ORBsupmed.L, IPL.R, SPG.R, THA.R, STG.R, IPL.R, IFGoperc.R) on PPMI. Statistical significance is denoted as follows: \*\*\* $p < 0.001$ , \*\* $p < 0.01$ , \* $p < 0.05$ , and ns  $p \geq 0.05$ .”

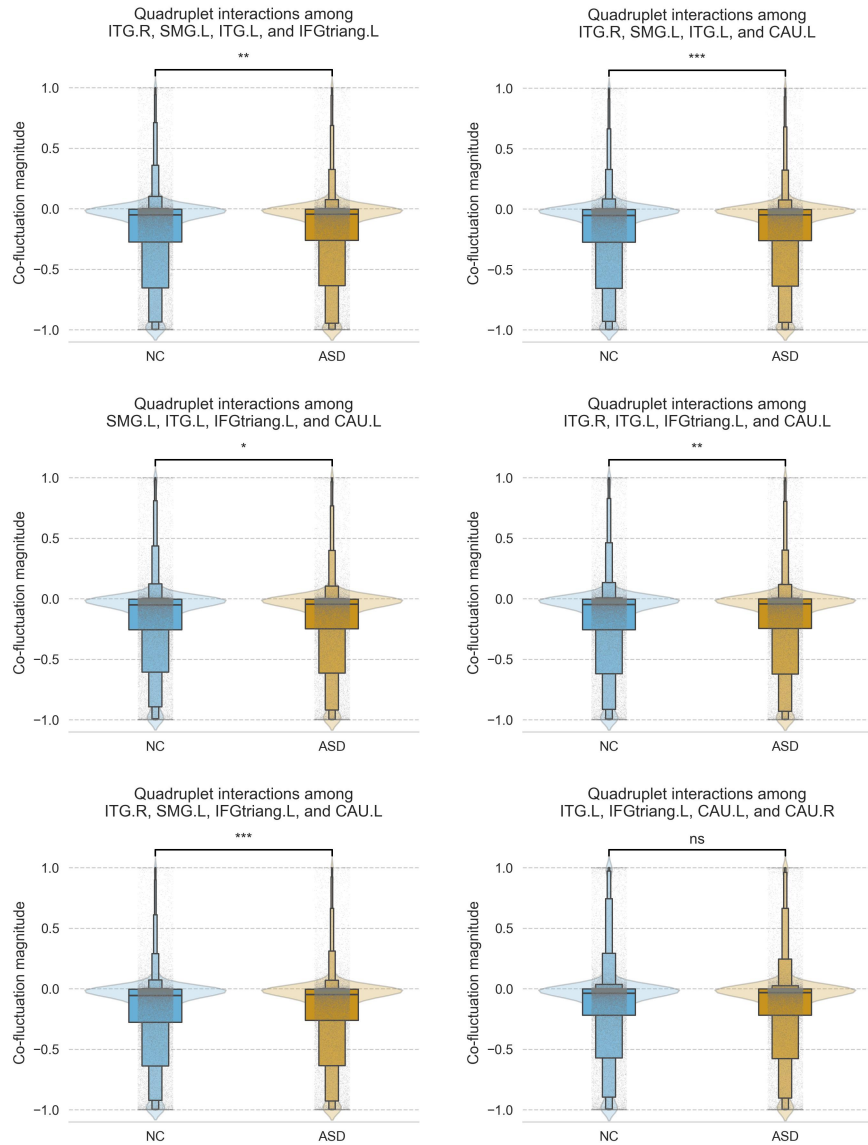


Figure 18: Group difference comparison of quadruplet interactions among the relevant brain regions (ITG.R, SMG.L, ITG.L, IFGtriang.L, CAU.L, and CAU.R) on ABIDE. Statistical significance is denoted as follows: \*\*\* $p < 0.001$ , \*\* $p < 0.01$ , \* $p < 0.05$ , and ns  $p \geq 0.05$ .”

network Transformer that integrates lower-order edge features with higher-order topological invariants. This new framework emphasizes the potential of quadruplet or higher-order region interactions — representing critical advancements for precision medicine, a deeper understanding of neurological disorders, and broader contributions to neuroimaging research. It demonstrates superior prediction accuracy for classifying Alzheimer’s Disease, Parkinson’s Disease, and Autism Spectrum Disorder compared to traditional machine learning models, graph neural network (GNN)-based models, Transformer-based models, hypergraph neural network (HGNN)-based models, and the Persistent Homology (PH)-based models. Additionally, ablation study also indicates that the effectiveness of quadruplet interactions compared to triplet interactions, the effectiveness of distinguishing between positively and negatively synergistic HOIs, and the effectiveness of different components in model.

The findings of our investigation revealed intriguing patterns. In the process of designing an orthonormal clustering readout for the identification of clusters of functionally similar nodes through soft clustering with orthonormal constraints, it was found that the assignment of nodes from different modes to distinct functional modules significantly improves classification accuracy. This finding indicates that both low-level and high-level feature patterns, which are frequently situated within different functional modular structures, are of paramount importance. This observation is in alignment with the conclusions reported in previous studies (Wang et al., 2019). This novel finding also provides a new opportunity for brain disease diagnostic models, specifically how to effectively identify and integrate low-order and higher-order patterns across different functional modules in the brain.

Furthermore, an investigation was conducted into the most discriminative neural patterns using an attention mechanism. This investigation revealed that quadruplet-level interaction signatures exhibit substantially greater importance than two-dimensional void descriptors and edge features in both the ADNI and ABIDE datasets. It is noteworthy that negative synergistic quadruplets tend to exhibit a higher degree of significance in comparison to their positive synergistic counterparts. Furthermore, positive synergistic voids have been observed to exceed negative synergistic voids in terms of their impact. This novel observation may offer critical insights into the pathological mechanisms underlying brain disorders. In order to provide further validation of these findings, inter-group comparisons were performed of signed higher-order topological signatures in the ADNI dataset. The find-

ings demonstrated a substantial discrepancy in the quantity of quadruplet-level interaction signatures among the groups ( $p < 0.001$ ) in comparison to void descriptors. Furthermore, positive voids demonstrated more pronounced inter-group disparities than negative voids. The findings suggest that disease progression may primarily disrupt higher-order neural interactions, which subsequently influence high-dimensional hole structures. An intriguing pattern emerged in the comparative analysis of CN individuals and those with AD. CN individuals appear to rely more on positive information for whole-brain topological organisation, whereas AD patients show a greater dependence on negative information. Furthermore, longitudinal trends indicate that the number of positive quadruplets gradually declines with disease progression, while negative quadruplets follow a biphasic trajectory – decreasing initially and then increasing. This suggests that during the transition from CN to MCI, there is a decline in both positive and negative synergistic interactions. However, as the condition progresses from MCI to AD, there is an increasing adoption of negative synergy by neural networks, alongside a suppression of excitability. This may be a compensatory mechanism employed by the brain to preserve functional integrity across neural modules. This finding aligns with the reference stating that excitatory neurons in the brains of Alzheimer’s patients suffer severe genomic damage (Miller et al., 2022).

In the context of investigating the significant brain regions and their interactions in the context of brain diseases, the utilisation of HOI-Brain facilitates the identification of these regions from a more comprehensive perspective, a departure from the low-level perspective that has been adopted in previous studies (Yan et al., 2019; Li et al., 2021). The findings, which function as potential biomarkers, are consistent with a substantial corpus of extant literature (Zidan et al., 2019; Zhi et al., 2024; Ye et al., 2019; Kim et al., 2021). Furthermore, they furnish novel insights with regard to the diagnosis of brain diseases. The right caudate has been identified as a potential hub node within the brain network. Previous literature has indicated that disruptions in this region are consistent with the progression of Alzheimer’s disease (Zhi et al., 2024). In a similar manner, the ITG.R has been observed to function as an additional pivotal hub within the brain network. It has been demonstrated that this region is selectively disrupted during the progression of ASD (Kim et al., 2021).

Furthermore, the higher-order organisational patterns identified by HOI-Brain offer novel insights into the diagnosis of brain diseases. Specifically,

the quadruplet interaction among CAU.R, HIP.L, PHG.R, and AMYG.L; the quadruplet interaction among OLF.L, HIP.L, PHG.R, and AMYG.L; and the quadruplet interaction among CAU.R, OLF.L, PHG.R, and AMYG.L, which involve the cortico-striatal-olfactory circuit, may serve as potential biomarkers for the early diagnosis of AD with p-values  $< 0.05$  during the progression from CN to MCI. It is noteworthy that the brain regions identified by HOI-Brain via the analysis of resting-state fMRI data are deemed to be of significant importance in the diagnosis of AD or ASD. This finding indicates that these brain regions may have sustained varying degrees of damage. However, HOIs exhibited by these regions demonstrate notable differences across various stages of disease progression. This finding is consistent with the conclusions of previous studies (Wang et al., 2019), suggesting a dissociation between HOIs in the brain and the functions of the individual brain regions themselves. Furthermore, observations were made concerning the transition from healthy individuals to those with AD or ASD. It was noted that the positive HOIs between relevant brain regions gradually weaken, indicating a progressive impairment of higher-order synergistic functions among brain regions. Conversely, the negative HOIs between these brain regions gradually strengthen, reflecting an increasing degree of internal functional disruption in the brain. This phenomenon is consistent with the findings reported in previous literature (Santoro et al., 2024). However, this phenomenon is exactly the opposite in Parkinson’s disease, which may be due to the fact that patients suffering from Parkinson’s disease, due to their motor impairments, are prone to hallucinations. Hallucinations in Parkinson’s disease may be attributable to an excessive influence of higher-order brain regions on early sensory processing. This is consistent with enhanced functional integration between sensory and higher-order networks (Tan et al., 2023).

## 6.2. Future work

Through our work, we have achieved good performance and interpretability in brain disease diagnosis. There are still some aspects worth exploring in the future. In this paper, we focus on the concordant signs of positive effects. However, exploring the influence of discordant signs of negative effects within the interpretable section, we found that these discordant signs may reflect redundant or conflicting information across multiple regions of the brain. Future work may investigate alternative methods to more explicitly address discordant patterns in the data. In addition, our model can reveal that these higher-order patterns evolve dynamically over time, so further investigation

into this temporal evolution could provide novel insights into disease progression. This opens up promising avenues for modeling the dynamic nature of brain network topology. Finally, our model demonstrates strong generalizability and can be adapted to other time series modalities—such as EEG or MEG—enabling further exploration of the importance of HOIs in the brain.

## 7. Conclusions

In summary, we propose a new framework, HOI-Brain (Higher-Order Interactions in Brain Network), which can accurately capture signed HOIs in brain networks, extract interpretable signed higher-order topological features, and further exploit the information between lower-order and higher-order features for brain disorder diagnosis. We applied HOI-Brain to datasets for Alzheimer’s disease, Parkinson’s disease, and Autism Spectrum Disorder. With the powerful interpretability, HOI-brain not only performs better on classification than 20 baselines, but also detects salient brain regions associated with classification and discovers important higher-order organizations. Overall, our model shows superiority over alternative graph learning and traditional machine learning classification models. By analyzing the attention maps of our multi-channel brain Transformer, our study identifies salient ROIs and their key interactions—from a whole-brain perspective—to distinguish brain disorders from healthy controls. Additionally, we uncover higher-order organizational patterns associated with specific disease progression stages. Notably, our framework is generalizable to the analysis of other neuroimaging time-series data. Our proposed framework demonstrates the potential of quadruplet or higher-order region interactions—critical advancements for precision medicine, enhanced understanding of neurological disorders, and broader contributions to neuroimaging research.

## 8. Declaration of Competing Interest

The authors declare that they have no known competing financial interests or personal relationships that could have appeared to influence the work reported in this paper.

## 9. Acknowledgements

This work was supported in part by the National Natural Science Foundation of China No.12471330 and the National Natural Science Foundation

of China No.12231018.

## References

- Adorjan, I., Ahmed, B., Feher, V., Torso, M., Krug, K., Esiri, M., Chance, S., Szele, F., 2017. Calretinin interneuron density in the caudate nucleus is lower in autism spectrum disorder. *Brain* 140.
- Baccini, F., Geraci, F., Bianconi, G., 2022. Weighted simplicial complexes and their representation power of higher-order network data and topology. *Phys. Rev. E* 106, 034319.
- Barrat, A., Barthelemy, M., Pastor-Satorras, R., Vespignani, A., 2004. The architecture of complex weighted networks. *Proceedings of the National Academy of Sciences of the United States of America* 101, 3747–52.
- Battiston, F., Cencetti, G., Iacopini, I., Latora, V., Lucas, M., Patania, A., Young, J.G., Petri, G., 2020. Networks beyond pairwise interactions: Structure and dynamics. *Physics Reports* 874, 1–92. Networks beyond pairwise interactions: Structure and dynamics.
- Bauer, U., 2021. Ripser: efficient computation of vietoris–rips persistence barcodes. *Journal of Applied and Computational Topology* 5.
- Bhattacharya, D., Kaur, R., Aithal, N., Sinha, N., Gregor Issac, T., 2025. Persistent homology for mci classification: a comparative analysis between graph and vietoris-rips filtrations. *Frontiers in Neuroscience* Volume 19 - 2025.
- Bi, F., Jia, Z., Lv, L., Zhang, Y., Zhu, C., Wan, C., 2025. Analysis of brain functional connectivity in children with autism spectrum disorder and sleep disorders: a fnirs observational study. *Frontiers in Psychology* 16.
- Bian, C., Xia, N., Xie, A., Cong, S., Dong, Q., 2023. Adversarially trained persistent homology based graph convolutional network for disease identification using brain connectivity. *IEEE transactions on medical imaging* PP.

- Bian, C., Xia, N., Xie, A., Cong, S., Dong, Q., 2024. Adversarially trained persistent homology based graph convolutional network for disease identification using brain connectivity. *IEEE Transactions on Medical Imaging* 43, 503–516.
- Bullmore, E., Sporns, O., 2009. Complex brain networks: Graph theoretical analysis of structural and functional systems. *Nature reviews. Neuroscience* 10, 186–98.
- Bv, M., Agrawal, A., 2022. Hippocampus and its involvement in alzheimer’s disease: a review. *3 Biotech* 12.
- Cassidy, B., Bowman, F.D., Rae, C., Solo, V., 2018. On the reliability of individual brain activity networks. *IEEE Transactions on Medical Imaging* 37, 649–662.
- Chelaru, M., Eagleman, S., Andrei, A., Milton, R., Kharas, N., Dragoi, V., 2021. High-order interactions explain the collective behavior of cortical populations in executive but not sensory areas. *Neuron* 109.
- Craddock, C., Benhajali, Y., Carlton, C., Francois, C., Evans, A., Jakab, A., Khundrakpam, B., Lewis, J., Qingyang, I., Michael, M., Chaogan, Y., Bellec, P., 2013. The neuro bureau preprocessing initiative: open sharing of preprocessed neuroimaging data and derivatives. *Frontiers in Neuroinformatics* 7.
- Dadi, K., Rahim, M., Abraham, A., Chyzhyk, D., Milham, M., Thirion, B., Varoquaux, G., 2019. Benchmarking functional connectome-based predictive models for resting-state fmri. *NeuroImage* 192.
- Delabays, R., De Pasquale, G., Dörfler, F., Zhang, Y., 2025. Hypergraph reconstruction from dynamics. *Nature Communications* 16.
- Echávarri, C., Aalten, P., Uylings, H., Jacobs, H., Visser, P., Gronenschild, E., Verhey, F., Burgmans, S., 2010. Atrophy in the parahippocampal gyrus as an early biomarker of alzheimer’s disease. *Brain structure & function* 215, 265–71.
- Esteban, O., Markiewicz, C.J., Blair, R.W., Moodie, C.A., Isik, A.I., Erramuzpe, A., Kent, J.D., Goncalves, M., DuPre, E., Snyder, M., Oya, H., Ghosh, S.S., Wright, J., Durnez, J., Poldrack, R.A., Gorgolewski, K.J.,

2019. fmriprep: a robust preprocessing pipeline for functional mri. *Nature methods* 16, 111—116.
- Faskowitz, J., Esfahlani, F., Jo, Y., Sporns, O., Betzel, R., 2020. Edge-centric functional network representations of human cerebral cortex reveal overlapping system-level architecture. *Nature Neuroscience* 23, 1–11.
- Fornito, A., Zalesky, A., Bullmore, E., 2016. *Fundamentals of Brain Network Analysis*. 1 ed., Academic Press, United States of America.
- Fotiadis, P., Parkes, L., Davis, K., Satterthwaite, T., Shinohara, R., Bassett, D., 2024. Structure–function coupling in macroscale human brain networks. *Nature Reviews Neuroscience* 25.
- Fugacci, U., Scaramuccia, S., Iuricich, F., Floriani, L.D., 2016. Persistent Homology: a Step-by-step Introduction for Newcomers, in: Pintore, G., Stanco, F. (Eds.), *Smart Tools and Apps for Graphics - Eurographics Italian Chapter Conference*, The Eurographics Association.
- Hamilton, W., Ying, Z., Leskovec, J., 2017. Inductive representation learning on large graphs, in: Guyon, I., Luxburg, U.V., Bengio, S., Wallach, H., Fergus, R., Vishwanathan, S., Garnett, R. (Eds.), *Advances in Neural Information Processing Systems*, Curran Associates, Inc.
- Hao, X., Li, J., Ma, M., Qin, J., Zhang, D., Liu, F., 2023. Hypergraph convolutional network for longitudinal data analysis in alzheimer’s disease. *Computers in Biology and Medicine* 168, 107765.
- Hu, J., Huang, Y., Dong, S., 2023. Transformer and snowball graph convolution learning for brain functional network analysis, in: *2023 IEEE International Conference on Bioinformatics and Biomedicine (BIBM)*, pp. 2809–2816.
- Hyekyoung, L., Chung, M., Kang, H., Kim, B., Lee, D., 2011. Discriminative persistent homology of brain networks. *Proceedings - International Symposium on Biomedical Imaging* , 841–844.
- Jie, B., Wee, C.Y., Shen, D., Zhang, D., 2016. Hyper-connectivity of functional networks for brain disease diagnosis. *Medical image analysis* 32, 84—100. doi:10.1016/j.media.2016.03.003.

- Kan, X., Cui, H., Lukemire, J., Guo, Y., Yang, C., 2022a. Fbnetgen: Task-aware gnn-based fmri analysis via functional brain network generation. *Proceedings of machine learning research* 172, 618—637.
- Kan, X., Dai, W., Cui, H., Zhang, Z., Guo, Y., Yang, C., 2022b. Brain network transformer, in: Koyejo, S., Mohamed, S., Agarwal, A., Belgrave, D., Cho, K., Oh, A. (Eds.), *Advances in Neural Information Processing Systems*, Curran Associates, Inc.. pp. 25586–25599.
- Kim, D., Lee, J., Jeong, B., Ahn, J., Kim, J., Lee, E., Kim, H., Lee, H.j., Han, C., 2021. Overconnectivity of the right heschl’s and inferior temporal gyrus correlates with symptom severity in preschoolers with autism spectrum disorder. *Autism Research* 14, 2314–2329.
- Kim, S., Lee, S.Y., Gao, Y., Antelmi, A., Polato, M., Shin, K., 2024. A survey on hypergraph neural networks: An in-depth and step-by-step guide, in: *Proceedings of the 30th ACM SIGKDD Conference on Knowledge Discovery and Data Mining*, Association for Computing Machinery, New York, NY, USA. p. 6534–6544.
- Kingma, D., Ba, J., 2014. Adam: A method for stochastic optimization. *International Conference on Learning Representations* .
- Kipf, T.N., Welling, M., 2017. Semi-supervised classification with graph convolutional networks, in: *International Conference on Learning Representations*.
- Kobayakawa, M., Tsuruya, N., Kawamura, M., 2016. Decision-making performance in parkinson’s disease correlates with lateral orbitofrontal volume. *Journal of the Neurological Sciences* 372.
- Li, M.g., Liu, T.f., Zhang, T.h., Chen, Z.y., Nie, B.b., Lou, X., Wang, Z.f., Ma, L., 2020. Alterations of regional homogeneity in parkinson’s disease with mild cognitive impairment: a preliminary resting-state fmri study. *Neuroradiology* 62.
- Li, X., Zhou, Y., Dvornek, N., Zhang, M., Gao, S., Zhuang, J., Scheinost, D., Staib, L., Ventola, P., Duncan, J., 2021. Braingnn: Interpretable brain graph neural network for fmri analysis. *Medical Image Analysis* 74, 102233.

- Lindquist, M.A., 2008. The statistical analysis of fmri data. *Statistical Science* 23, 439–464.
- Luo, X., Wu, J., Yang, J., Xue, S., Beheshti, A., Sheng, Q.Z., McAlpine, D., Sowman, P., Giral, A., Yu, P.S., 2024. Graph neural networks for brain graph learning: A survey, in: Larson, K. (Ed.), *Proceedings of the Thirty-Third International Joint Conference on Artificial Intelligence, IJCAI-24, International Joint Conferences on Artificial Intelligence Organization*. pp. 8170–8178. Survey Track.
- Luo, Y., Chen, Q., Li, F., Yi, L., Xu, P., Zhang, Y., 2025. Hierarchical feature extraction on functional brain networks for autism spectrum disorder identification with resting-state fmri data. *Neural Networks* 188, 107450.
- Miller, M., Huang, A., Kim, J., Zhou, Z., Kirkham, S., Maury, E., Ziegenfuss, J., Reed, H., Neil, J., Rento, L., Ryu, S., Ma, C., Luquette, L., Ames, H., Oakley, D., Frosch, M., Hyman, B., Lodato, M., Lee, E., Walsh, C., 2022. Somatic genomic changes in single alzheimer’s disease neurons. *Nature* 604, 1–9.
- Neuhäuser, L., Mellor, A., Lambiotte, R., 2020. Multibody interactions and nonlinear consensus dynamics on networked systems. *Physical Review E* 101.
- Paszke, A., Gross, S., Chintala, S., Chanan, G., Yang, E., DeVito, Z., Lin, Z., Desmaison, A., Antiga, L., Lerer, A., 2017. Automatic differentiation in pytorch, in: *NIPS-W*.
- Pedregosa, F., Varoquaux, G., Gramfort, A., Michel, V., Thirion, B., Grisel, O., Blondel, M., Prettenhofer, P., Weiss, R., Dubourg, V., Vanderplas, J., Passos, A., Cournapeau, D., Brucher, M., Perrot, M., Duchesnay, E., 2011. Scikit-learn: Machine learning in Python. *Journal of Machine Learning Research* 12, 2825–2830.
- Petri, G., Expert, P., Turkheimer, F., Carhart-Harris, R., Nutt, D., Hellyer, P., Vaccarino, F., 2014. Homological scaffolds of brain functional networks. *Journal of The Royal Society Interface* 11, 20140873.
- Santoro, A., Battiston, F., Lucas, M., Petri, G., Amico, E., 2024. Higher-order connectomics of human brain function reveals local topological sig-

- natures of task decoding, individual identification, and behavior. *Nature Communications* 15.
- Santoro, A., Battiston, F., Petri, G., Amico, E., 2023. Higher-order organization of multivariate time series. *Nature Physics* 19, 1–9.
- Shine, J.M., Koyejo, O., Bell, P.T., Gorgolewski, K.J., Gilat, M., Poldrack, R.A., 2015. Estimation of dynamic functional connectivity using multiplication of temporal derivatives. *NeuroImage* 122, 399–407.
- Sizemore, A., Giusti, C., Kahn, A., Vettel, J., Betzel, R., Bassett, D., 2018. Cliques and cavities in the human connectome. *Journal of Computational Neuroscience* 44, 1–31.
- Sporns, O., 2010. *Networks of the Brain*. The MIT Press.
- Su, S., Duta, I., Magister, L.C., Liò, P., 2024. Explaining hypergraph neural networks: From local explanations to global concepts. URL: <https://arxiv.org/abs/2410.07764>, arXiv:2410.07764.
- Talesh Jafadideh, A., Mohammadzadeh Asl, B., 2022. Topological analysis of brain dynamics in autism based on graph and persistent homology. *Computers in Biology and Medicine* 150, 106202.
- Tan, J.B., Müller, E.J., Orlando, I.F., Taylor, N.L., Margulies, D.S., Szeto, J., Lewis, S.J.G., Shine, J.M., O’Callaghan, C., 2023. Abnormal higher-order network interactions in parkinson’s disease visual hallucinations. *Brain* 147, 458–471.
- Tzourio-Mazoyer, N., Landeau, B., DF, P., Crivello, F., Etard, O., Delcroix, N., Mazoyer, B., Marc, J., 2002. Automated anatomical labeling of activations in spm using a macroscopic anatomical parcellation of the mni mri single-subject brain. *NeuroImage* 15, 273–89.
- Vaccarino, F., Fugacci, U., Scaramuccia, S., 2022. *Persistent Homology: A Topological Tool for Higher-Interaction Systems*. Springer International Publishing, Cham. pp. 97–139.
- Veličković, P., Cucurull, G., Casanova, A., Romero, A., Liò, P., Bengio, Y., 2018. Graph attention networks, in: *International Conference on Learning Representations*.

- Wang, M., Huang, J., Liu, M., Zhang, D., 2021. Modeling dynamic characteristics of brain functional connectivity networks using resting-state functional mri. *Medical Image Analysis* 71, 102063.
- Wang, R., Lin, P., Liu, M., Wu, Y., Zhou, T., Zhou, C., 2019. Hierarchical connectome modes and critical state jointly maximize human brain functional diversity. *Phys. Rev. Lett.* 123, 038301.
- Wang, W., Xiao, L., Qu, G., Calhoun, V., Wang, Y.P., Sun, X., 2024a. Multiview hyperedge-aware hypergraph embedding learning for multisite, multiatlas fmri based functional connectivity network analysis. *Medical Image Analysis* 94, 103144.
- Wang, X., Shen, Y., Wei, W., Bai, Y., Li, P., Ding, K., Zhou, Y., Xie, J., Zhang, X., Guo, Z., Wang, M., 2024b. Alterations of regional homogeneity and functional connectivity in different hoehn and yahr stages of parkinson’s disease. *Brain Research Bulletin* 218, 111110.
- Wang, X., Xin, J., Wang, Z., Li, C., Wang, Z., 2022. An evolving hypergraph convolutional network for the diagnosis of alzheimer’s disease. *Diagnostics* 12, 2632.
- Xia, J., Chan, Y., Girish, D., Rajapakse, J., 2025. Interpretable modality-specific and interactive graph convolutional network on brain functional and structural connectomes. *Medical Image Analysis* 102, 103509.
- Xia, M., Wang, J., He, Y., 2013. Brainnet viewer: A network visualization tool for human brain connectomics. *PLoS ONE* 8, e68910. doi:10.1371/journal.pone.0068910.
- Xiao, L., Wang, J., Hosseinzadeh Kassani, P., Zhang, Y., Bai, Y., Stephen, J., Wilson, T., Calhoun, V., Wang, Y.P., 2019. Multi-hypergraph learning based brain functional connectivity analysis in fmri data. *IEEE Transactions on Medical Imaging* PP, 1–1.
- Xu, J., Wang, C., Xu, Z., Li, T., Chen, F., Chen, K., Gao, J., Hu, Q., 2019. Specific functional connectivity patterns of middle temporal gyrus subregions in children and adults with autism spectrum disorder. *Autism Research* 13, 410–422.

- Xu, J., Yang, Y., Huang, D., Gururajapathy, S.S., Ke, Y., Qiao, M., Wang, A., Kumar, H., McGeown, J., Kwon, E., 2023. Data-driven network neuroscience: On data collection and benchmark, in: Oh, A., Naumann, T., Globerson, A., Saenko, K., Hardt, M., Levine, S. (Eds.), *Advances in Neural Information Processing Systems*, Curran Associates, Inc.. pp. 21841–21856.
- Yan, Y., Zhu, J., Duda, M., Solarz, E., Sripada, C.S., Koutra, D., 2019. Groupinn: Grouping-based interpretable neural network for classification of limited, noisy brain data. *Proceedings of the 25th ACM SIGKDD International Conference on Knowledge Discovery & Data Mining* .
- Ye, C., Mori, S., Chan, P., Ma, T., 2019. Connectome-wide network analysis of white matter connectivity in alzheimer’s disease. *NeuroImage: Clinical* 22, 101690.
- Ying, C., Cai, T., Luo, S., Zheng, S., Ke, G., He, D., Shen, Y., Liu, T.Y., 2021. Do transformers really perform badly for graph representation?, in: Ranzato, M., Beygelzimer, A., Dauphin, Y., Liang, P., Vaughan, J.W. (Eds.), *Advances in Neural Information Processing Systems*, Curran Associates, Inc.. pp. 28877–28888.
- Yoshimura, N., Kawamura, M., Masaoka, Y., Homma, I., 2005. The amygdala of patients with parkinson’s disease is silent in response to fearful facial expressions. *Neuroscience* 131, 523–34.
- Yu, S., Jin, S., Li, M., Sarwar, T., Xia, F., 2024. Long-range brain graph transformer, in: Globerson, A., Mackey, L., Belgrave, D., Fan, A., Paquet, U., Tomczak, J., Zhang, C. (Eds.), *Advances in Neural Information Processing Systems*, Curran Associates, Inc.. pp. 24472–24495.
- Zhang, Z., Aggarwal, V., Angelov, P., Jiang, R., 2025. Modeling brain aging with explainable triamase vit: Towards deeper insights into autism disorder. *IEEE journal of biomedical and health informatics* PP.
- Zheng, K., Yu, S., Chen, L., Dang, L., Chen, B., 2024. Bpi-gnn: Interpretable brain network-based psychiatric diagnosis and subtyping. *NeuroImage* 292, 120594.
- Zhi, Y., Huang, T., Liu, S., Li, M., Hu, H., Liang, X., Jiang, Z., Zhu, J., Liu, R., 2024. Correlation between iron deposition and cognitive function in

mild to moderate alzheimer's disease based on quantitative susceptibility mapping. *Frontiers in Aging Neuroscience* 16.

Zhu, X.W., Zhang, L.L., Zhu, Z.M., Wang, L.Y., Ding, Z., Fang, X.M., 2022. Altered intrinsic brain activity and connectivity in unaffected parents of individuals with autism spectrum disorder: a resting-state fmri study. *Frontiers in Human Neuroscience* 16, 997150.

Zidan, M., Boban, J., Bjelan, M., Todorović, A., Vujanic Stankov, T., Semnic, M., Boban, N., Kozic, D., 2019. Thalamic volume loss as an early sign of amnesic mild cognitive impairment. *Journal of Clinical Neuroscience* 68.

Zirh, T., Lenz, F., Reich, S., Dougherty, P., 1998. Patterns of bursting occurring in thalamic cells during parkinsonian tremor. *Neuroscience* 83, 107–21.

Zou, T., Chen, C., Chen, H., Wang, X., Gan, L., Wang, C., Gao, Q., Zhang, C., Liao, W., Cheng, J., Li, R., 2024. Structural-functional connectivity decoupling in multiscale brain networks in parkinson's disease. *BMC Neuroscience* 25.

## Appendix A. Persistent Homology Theory

### Appendix A.1. Basic Concepts in Algebraic Topology

For related basic concepts about Persistent Homology theory, please refer to the following references (Fugacci et al., 2016; Vaccarino et al., 2022).

**Definition 3. (*Simplex*)** Given affinely independent points  $v_0, v_1, \dots, v_k$  in  $\mathbb{R}^d$ , a  $k$ -simplex  $\sigma = [v_0, v_1, \dots, v_k]$  is the convex hull of these points. A face of  $\sigma$  is any simplex  $\tau$  spanned by a nonempty subset of its vertices. Geometrically, a 0-simplex represents a point, a 1-simplex represents an edge, a 2-simplex represents a triangle (including interior), and a 3-simplex represents a quadruplet (solid).

**Definition 4. (*Simplicial Complex*)** An abstract simplicial complex  $\mathcal{K}$  on a finite vertex set  $V$  is a collection of some non-empty subsets of  $V$  satisfying:

1. For every  $v \in V$ , the singleton  $\{v\}$  belongs to  $\mathcal{K}$ .
2. If  $\sigma \in \mathcal{K}$  and  $\tau \subseteq \sigma$  is a non-empty subset, then  $\tau \in \mathcal{K}$ .

Each element  $\sigma \in \mathcal{K}$  is called a simplex and  $\tau$  is called the face of  $\sigma$ . A simplex with  $|\sigma| = k + 1$  vertices is a  $k$ -simplex, representing a  $k$ -order interaction.

**Definition 5. (*Chain Group*)** The  $k$ -chain group  $C_k$  is the free abelian group generated by oriented  $k$ -simplices. An element  $c \in C_k$  is a formal sum  $c = \sum a_i \sigma_i$  with  $a_i \in \mathbb{Z}$ .

**Definition 6. (*Boundary Operator*)** The linear operator  $\partial_k : C_k \rightarrow C_{k-1}$  acts on a  $k$ -simplex  $\sigma = [v_0, \dots, v_k]$  as:

$$\partial_k(\sigma) = \sum_{i=0}^k (-1)^i [v_0, \dots, \hat{v}_i, \dots, v_k]$$

where  $\hat{v}_i$  denotes vertex removal. The fundamental property is  $\partial_k \circ \partial_{k+1} = 0$ .

**Definition 7. (*Homology Group*)** The  $k$ -homology group is the quotient:

$$H_k = \ker \partial_k / \text{im } \partial_{k+1}$$

Elements of  $\ker \partial_k$  are cycles (closed structures). Elements of  $\text{im } \partial_{k+1}$  are boundaries (trivially closed structures).

Homology groups provide a mathematical characterization of topological features in a shape. Formally, for each dimension  $k$ , the  $k$ -th Betti number  $\beta_k = \text{rank } H_k(\mathcal{K})$  enumerates the independent non-boundary  $k$ -dimensional cycles in the simplicial complex  $\mathcal{K}$ . These Betti numbers have concrete geometric interpretations:  $\beta_0$  counts the connected components;  $\beta_1$  counts independent 1-dimensional loops (e.g., holes/tunnels);  $\beta_2$  counts enclosed cavities bounded by 2D surfaces.

### *Appendix A.2. Persistent Homology*

**Persistent Homology:** Persistent homology is an important tool in topological shape analysis, which aims at overcoming intrinsic limitations of classical homology by allowing for a multi-scale approach to shape description. In a nutshell, persistent homology describes the changes in homology that occur to an object which evolves with respect to a parameter.

Given a simplicial complex  $\mathcal{K}$ , a *filtration* of  $\mathcal{K}$  is a finite sequence of subcomplexes  $\mathcal{K}^f := \{\mathcal{K}^p \mid 0 \leq p \leq m\}$  of  $\mathcal{K}$  such that:

$$\emptyset = \mathcal{K}^0 \subseteq \mathcal{K}^1 \subseteq \dots \subseteq \mathcal{K}^m = \mathcal{K}$$

For indices  $p, q \in \{0, \dots, m\}$  with  $p \leq q$ , the  $(p, q)$ -persistent  $k$ -homology group  $H_k^{p,q}(\mathcal{K}^f)$  consists of the  $k$ -cycles included from  $C_k(\mathcal{K}^p)$  into  $C_k(\mathcal{K}^q)$  modulo boundaries. Formally, it is defined as:

$$H_k^{p,q}(\mathcal{K}^f) := \text{Im}(i_k^{p,q})$$

where  $i_k^{p,q} : H_k(\mathcal{K}^p) \rightarrow H_k(\mathcal{K}^q)$  denotes the linear map induced by the inclusion  $\mathcal{K}^p \hookrightarrow \mathcal{K}^q$ .

Crucially, persistent homology enriches classical homology by quantifying feature persistence across scales. Whereas classical homology identifies non-boundary cycles at a single scale, persistent homology captures cycles that emerge as non-boundaries at filtration stage  $p$  and subsequently become boundaries at stage  $q > p$ . The interval  $(p, q)$ , termed the *persistence* of the cycle, provides a quantitative measure of its topological significance within the shape.

**Definition 8.** (*2-dimensional void*) A 2-dimensional void corresponds to a non-boundary 2-cycle in  $H_2$ . Geometrically, it is an enclosed void bounded by a surface of triangles. For a simplicial complex  $\mathcal{K}$ :

- **Birth:** When a set of triangular faces forms a closed surface.

- **Death:** When the void is filled by a chain of 3-simplices (quadruplet).

The persistence  $\text{pers}(b, d) = d - b$  quantifies topological significance, where  $b$  denotes the birth (or appearance) weight of a topological feature (e.g., the weight of last triangular face forming a closed surface), and  $d$  denotes the death (or disappearance) weight of that feature (e.g., when a quadruplet fills the void).

## Appendix B. Ablation Study of Higher-Order Features on PPMI and Taowu Datasets

To evaluate the effectiveness of more complex signed quadruplet structures and voids (2D holes) formed by triangular faces, we report here a performance comparison with varying feature combinations on the TaoWu and PPMI datasets to have more insight into how HOI-Brain performs on different tasks.

Table B.8: Performance comparison with varying combinations of features on the TaoWu datasets (%). The best results are marked in bold.

Method	Taowu			
	Accuracy	Precision	Recall	F1-score
edge	65.0±5.0	<u>84.8±18.9</u>	55.0±36.7	54.6±17.9
edge+violating triangles+1D loops	70.0±16.9	63.3±37.1	60.0±33.9	60.2±32.9
edge+violating triangles+good quadruplets	67.5±16.9	57.4±33.7	<u>75.0±38.7</u>	62.8±32.4
edge+1D loops+2D voids	67.5±17.0	79.8±17.5	60.0±25.5	62.3±12.8
edge+good quadruplets+2D voids	<b>77.5±9.3</b>	<b>89.3±13.7</b>	70.0±29.1	<u>72.2±17.8</u>
edge+signed good quadruplets+signed 2D voids	<u>77.5±12.3</u>	82.4±9.3	<b>77.5±12.3</b>	<b>75.9±13.9</b>

Table B.9: Performance comparison with varying combinations of features on the PPMI datasets (%). The best results are marked in bold.

Method	PPMI			
	Accuracy	Precision	Recall	F1-score
edge	61.4±7.4	<u>71.6±18.7</u>	45.1±10.1	53.5±8.9
edge+violating triangles+1D loops	57.6±2.4	64.0±9.2	43.8±13.9	49.4±8.1
edge+violating triangles+good quadruplets	60.5±9.2	66.5±19.7	56.4±12.0	58.7±8.3
edge+1D loops+2D voids	63.3±4.2	69.8±11.2	56.9±18.4	59.6±6.1
edge+good quadruplets+2D voids	<u>65.2±4.3</u>	<b>73.1±12.2</b>	<u>58.7±11.1</u>	<u>63.7±4.5</u>
edge+signed good quadruplets+signed 2D voids	<b>66.1±4.0</b>	69.0±4.0	<b>66.3±4.2</b>	<b>64.7±4.7</b>

## Appendix C. Results of Hyperparameter Analysis on Other Metrics

In the hyperparameter analysis section, we only reported the influence of the key hyperparameter, the number of clusters, based on the accuracy metric. To better evaluate the impact of this hyperparameter, we additionally present the results of hyperparameter analysis for the other three metrics: precision, recall, and F1 score.

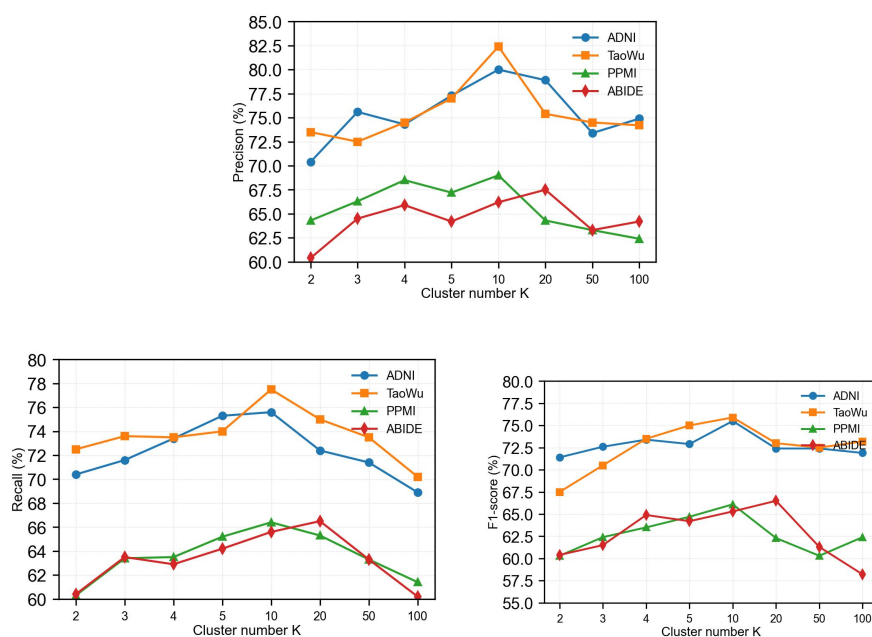


Figure C.19: Influence of the key hyper-parameter, the number of clusters, for model performance on other three metrics.